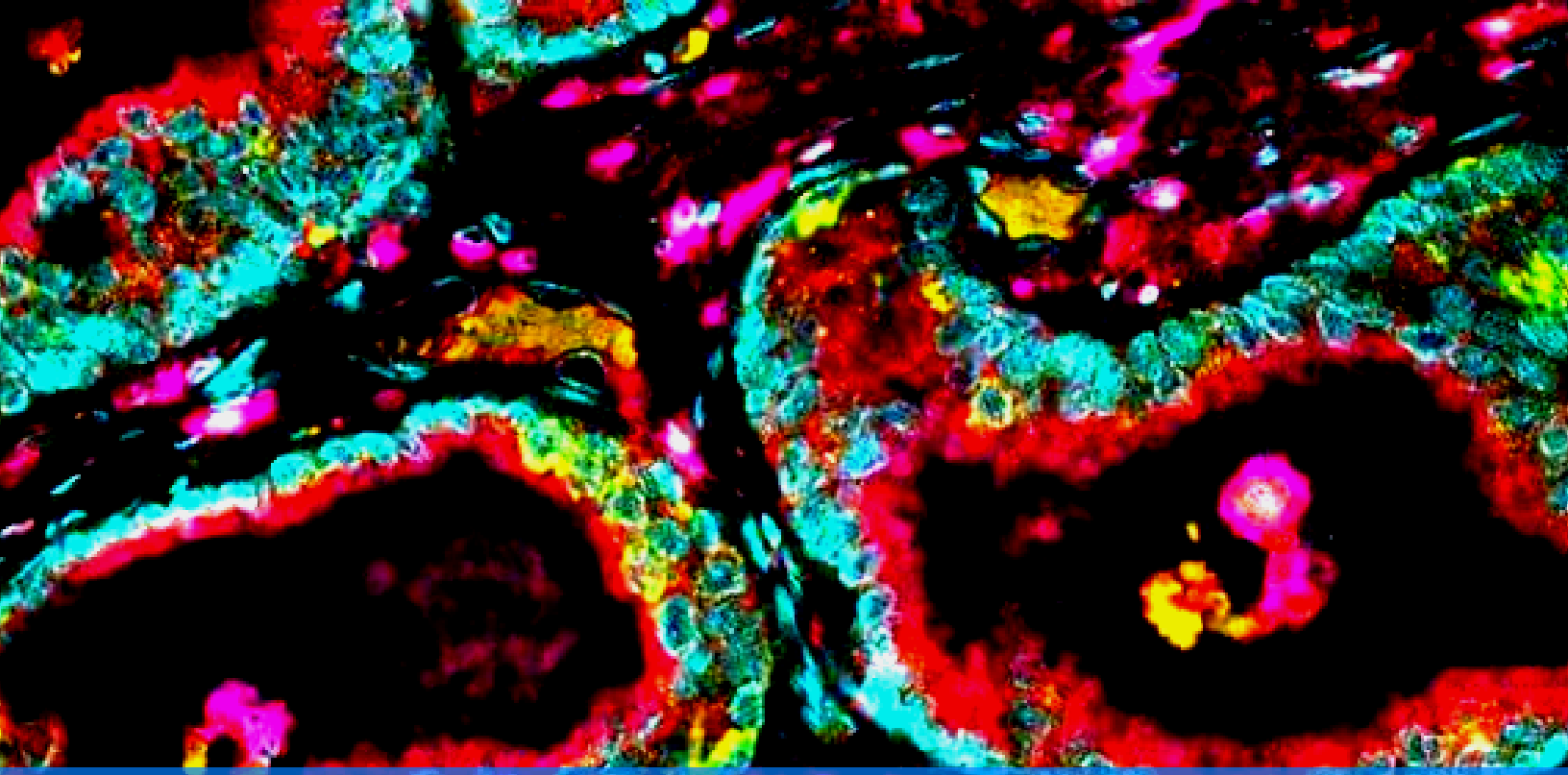

ΣIGMA

VOL. 4 SPRING 2017

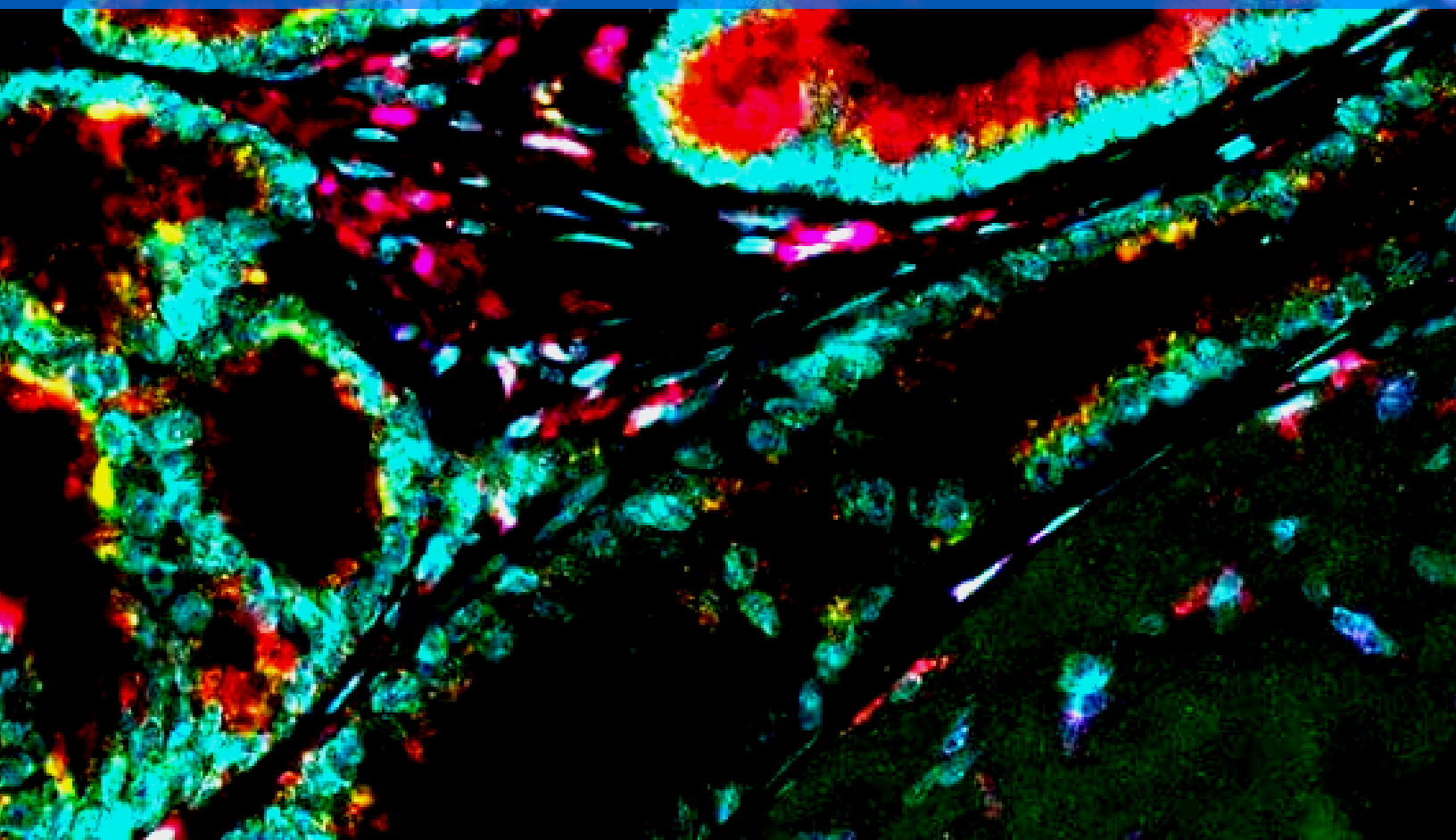

Welcome to the Research Club!

The Research Club is created to facilitate student research in a myriad of topics. Every Friday, we will either be listening to a guest speaker, doing experiments, learning lab techniques, or working on internship applications. It is one of the few clubs in Stuyvesant dedicated to developing student's interest in research and preparing student's for greater opportunities. One of its main goals is to revive Sigma, its magazine, in order for more members of the Stuyvesant community to have access to scientific material written by their peers. By encouraging its members to write articles, the club aims to hone the writing skills of future scientists.

Additionally, the club will expand and strive to compete in science competitions by forming members into teams based on their interests and levels of experience. The club hopes to motivate its members to actively engage in scientific discussions and earn valuable experience by receiving feedback to improve their scientific writing and teamwork.

Sub-headings

Take Advantage of this Edition

This edition features many of this year's graduating seniors' research reports, which were submitted to Regeneron and various other prestigious competitions.

The reports have been annotated and shortened by members the Research Club. We hope this can aid your understanding of the report.

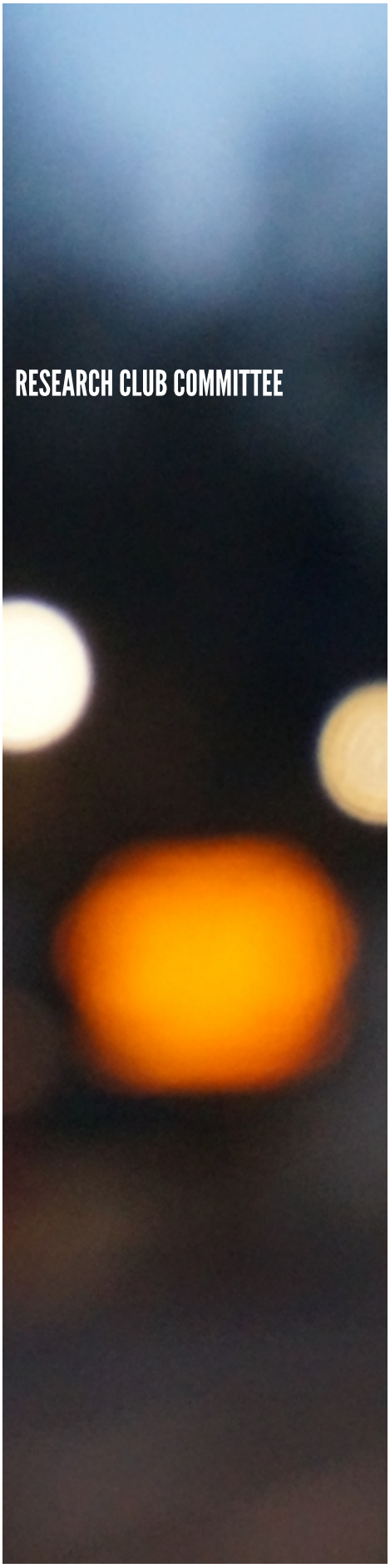

Faculty Advisor
Jason Econome

Faculty Advisor
Scott Thomas

Student Leadership Board

President
Kimberly Ho

Vice President
Benedict Ho

Editor in Chief
Alvin Zhu

Editor in Chief
Janny Chen

Layout Manager
Jialin Chen

Layout Manager
Julia Lu

Information and Design Architect
Julie Wu

Information and Design Architect
Annie Li

Information and Design Architect
Jennifer Lu

Student Research Coordinator
Marie Ivantechenko

Student Leadership Board in Training

Marie Ivantechenko

Alexandra Wen

Julian Rubinfein

Kent Dong

Lauren Mei

Bhavin Tanna

Heyu Li

Special thanks for the support of Principal Contreras, the Biology Department, the Chemistry & Physics Department, Alumni Association, and the Student Union.

Table of Contents

Special Guest Speaker ... Vanessa Liu

Written by Lauren Mei, Alexander Radu, Kent Dong

Liu was a previous Intel Finalist and alumni of Stuyvesant High School, and later went on to attend Harvard University. She is currently focused on media and marketing.

Question #1: How did you become interested in Science at Stuy?

Answer: I was lucky to have a great mentor who worked me to improve my skills of asking questions and making inquiries about various scientific processes.

Question #2: Can you elaborate on how you build up a relationship with your mentor?

Answer: Building up a relationship takes time and effort and I remember sitting down with my mentor and setting a goal for what I was going to do as well as asking if I could help him with his work.

Question #3: Can you describe the process of finding your lab?

Answer: The main thing about finding a lab is to be broad in scope. This widens the possibility og getting into a lab that will be as close to your interest as possible. Highly specialized labs are uncommon and there may be only one or two in the entire country. Be persistent in your search for a lab, and take the initiative to build understanding with your potential mentor before them meeting them. Lastly, be genuinely interested and don't give up if you get rejected from a few labs!

Question #4: If you can ever redo anything during your research experience, what will you do?

Answer: Surprisingly, there is nothing that I want to redo. Every mistakes I've made helped me to become a better researcher. It may hurt at first, but with determination, the harm can be reversed and you will only increase in understanding. However, one thing that I would like to take more advantage of during my research experience is talking to the grad students in my lab. I was too focused on my own work to pay attention to those of others around me -- who knows, maybe I would have found something interesting, or even better my own experiment!

Question #5: If you have all the money in the world to advance a scientific field, what will it be?

Answer: I am fascinated by the human brain. Take for instance, the story of a young woman who predicted her own death during the pregnancy, and as a result was able to prevent herself from dying of bloodless. (For the whole story, please read the book 37 Seconds by Stephanie Arnold -- 37 seconds refer to the time she was pronounced dead). There is so little we know about our own brain, and if we are to unlock its potential, we can do so much more.

Characterization of a new target for tuberculosis therapy by identifying a gene responsible for resistance to two anti-tuberculosis compounds in Mycobacterium smegmatis

Raphael Kirou

Annotated by Kent Dong

Introduction

Tuberculosis is the deadliest human infectious disease, killing 1.5 million people each year1. Although several drugs kill Mycobacterium tuberculosis (Mtb), resistant mutants have emerged as a global public health problem. In order to identify new drugs against tuberculosis, compound libraries have been screened for anti-tuberculosis activity. In this study, two similar anti-tuberculosis compounds, Compounds 1A and 1B, were tested against Mycobacterium smegmatis (Msm) as a proxy to Mtb. Strains resistant to the compounds were then studied for genetic mutations.

Substitute

In this study, msm mycobacteria are used as a proxy to tuberculosis, due to it nonpathogenic nature and reproduction rate. Msm cultures that grew despite exposure to high concentrations of the drugs were then analyzed for gene mutations. Gene YMsm, was found to a carry a novel mutation in resistant Msm strains to Compound 1A. This data suggests that the two compounds target Gene YMsm in killing the cells and hopefully will facilitate the development of new, alternate, less harmful drugs targeting Gene YMtb.

Methods

The first part of the project entailed isolating a large number of Msm mutants resistant to two compounds (Compound 1A and Compound 1B), and Wild type Msm was plated onto 7H11 agar. The Minimum Inhibitory Concentration (MIC90) of wild type Msm is 0.75 μM for both Compounds 1A and 1B, based on previous experiments. This was used as a basis for making plates. Wild type Msm was streaked on all of the plates. After they were incubated for three days, the number of colonies that grew in each plate was counted to calculate the Frequency of Resistance (FOR).

In microbiology, the minimum inhibitory concentration (MIC) is the lowest concentration of a chemical that prevents visible growth of a bacterium (in other words, at which it has bacteriostatic activity)

Normal

The FOR is calculated by dividing the number of colonies grown by the number of cells plated (Table 1).

A detergent to help prevent clumping.

56 candidate mutants were re-streaked onto new plates with the same concentrations as the parent plates to confirm their resistance. If there is resistance, they are grown in liquid culture containing glycerol, and a 0.02% concentration of tyloxapol. The mutants A3, B4, C1, D4, E1, F8, G4, and H2 were chosen for further testing based on abnormal colony morphology (Table 1). Next, the phenotypes of the eight principal mutants were tested on agar without any compound. Then, the small number of cells remaining on the pipette tip was punctured into the swarming agar (Figures 2A and 2B). Then, they were left to shake in the incubator. The OD580 of each culture was measured at several times between the start and end time (24 hours).(Figure 3).

This is because differences in colony morphology may signal cell wall defects, which are often apparent by phenotype.

Swarming agar is used to highlight the motility of bacteria in semi-solid media

Absorbance level

Another phenotypic experiment entailed finding the Minimum Inhibitory Concentrations (MICs) of the eight principal mutants and wild type under Compound 1A. The MICs were found by using nine 96-well (8 X 12) plates for our mutants and wild type. The plates were shaken in the incubator for 48 hours. The results are shown in (Figures 4 and 5). In order to carry out genotypic analysis on our mutants, genomic DNA had to be extracted from the cells using a two-day chromosomal DNA preparation procedure.

The first step entailed making a TE Buffer solution.500 mL water, 0.788 g TRIS Hydrochloride, and 0.18612 g EDTA (Ethylenediaminetetraacetic acid disodium salt dihydrate). The solution was adjusted to a pH of 8. The solution is centrifuged, the supernatant discarded and pellet lysed using lysozyme, and then incubated at 37 celsius overnight. Cold chloroform were added to the cultures and vortexed for 2 times.

Chloroform collected on the bottom and DNA in an aqueous phase collected on the top, separated by a thin layer of cell residue (proteins and lipids).

Then, 420 µL isopropanol and 10 µL 3M sodium acetate were added to the samples. The content are centrifuged, supernatant discarded, and pellet lysed and air-dried. The DNA concentration was measured with a nanodrop machine and then diluted to 100 ng/µL.

These new solutions were stored at -80C and used in further experiments.

Finally, the genes responsible for causing resistance to the compounds in mutants were targeted. Polymerase Chain Reaction (PCR) was used to amplify the two genes suspected of being mutated (Gene XMsm and Gene YMsm). The samples were split up into 5 PCR tubes so that a gradient of annealing temperatures could be tested.

A small amount of each reaction was loaded on an agarose gel (0.5 g agarose, 50 mL TAE, 6 µL ethidium bromide) to check if the PCR was successful. If it was, PCR purification was used on the remaining PCR product not used in the gel using a DNA purification kit. The concentration of the liquid in ng/µL was then measured for each solution using a nanodrop machine. Samples were sent to Macrogen USA along with primers for sequencing.

Results

One of the mutants, B4, showed a clear difference in morphology compared to the other mutants and wild type when grown on two different 7H11 agar plates (Figures 1A and 1B). The colony looked flat; this stood in contrast to the other colonies, which looked ruffled (a characteristic stemming from the fact that Msm cells often grow on top of each other). This difference could signal slower growth and/or a cell wall defect. In liquid media, B4 did not show a significant difference in growth (Figure 3),

The mutant genotypes were analyzed through DNa extraction, PCR, and sequencing. One mutant, D4, was found to carry a mutation in Gene YMsm. The mutation was a single nucleotide substitution that resulted in a proline to leucine amino acid change (P76L) in the gene product (Figure 6). (Figure 8) shows differences in protein structures. In addition, mutant D4 showed complete resistance up to 100 µM of Compound 1A (Figure 4), while the other mutants were eventually inhibited.

In this study, 56 Msm mutants resistant to Compounds 1A and 1B were isolated. Based on colony morphology on 7H11 agar, eight mutants were chosen for further experiments. Out of these eight mutants, one of them (B4) showed a striking difference in colony morphology on 7H11 agar. Finally, the DNA of the eight mutants was extracted for use in PCR. PCR amplification and sequencing for Gene YMsm in Mutant D4 showed a nucleotide substitution.

This change resulted in a proline to leucine amino acid change in the gene's product that seems to have altered the binding pocket of Protein Y and thus perhaps prevented the binding of Compound 1A.

s The identification of the Gene YMsm mutation provides evidence that this gene's product is probably the target of these anti-tuberculosis compounds. Furthermore, the predicted conformational change in the protein's structure from the mutation in Gene YMsm demonstrates the potential functional significance of the mutation and supports the notion that this protein is the target.

Conclusion

Possible further experiments to be done include testing of more Msm mutants for Gene YMsm, but also for Gene XMsm mutations. In addition, experiments could be done to confirm that the mutation in Gene YMsm is indeed the cause of resistance to Compound 1A. This study addresses a pressing need for new antibiotics against tuberculosis, a global public health problem. Combining drugs with anti-tuberculosis activity under both proliferating and stress conditions will hopefully lead to shorter and more efficient treatment regimens for tuberculosis.

All Figures are Shown Below

Table 1: **Isolation of mutants resistant to Compounds 1A**

Concentration of Compound	3.75 µM Compound 1A		7.5 µM Compound 1A			15 µM Compound 1A		7.5 µM Compound 1B	
Number of Msm cells	10^7	10^8	10^7	10^8	10^9	10^8	10^9	10^7	10^8
Frequency of resistance	4.5×10^{-6}	5.1×10^{-6}	3.2×10^{-6}	3.4×10^{-6}	*Too many to count	2.6×10^{-6}	*Too many to count	2.0×10^{-6}	3.2×10^{-6}
Names given to candidate mutants	A1 – A8 A3	B1 – B8 B4	C1 – C4 C1	D1 – D8 D4	E1 – E4 E1	F1 – F8 F8	G1 – G8 G4	H1 – H4 H2	H5 – H8

The table above shows the initial concentrations of compound and number of wild type Msm cells used to produce mutants. As a note, the actual numbers of cells used were 5.3*106 cells, 5.3*107 cells, and 5.3*108 cells, as found by CFU of the inoculum. These values were used in the Frequency of Resistance calculations below. Frequency of resistance is calculated as the number of resistant colonies divided by the number of cells originally used. Mutants in red were chosen for further study.

Mutant B4 shows unique colony morphology when grown

Figure 1A

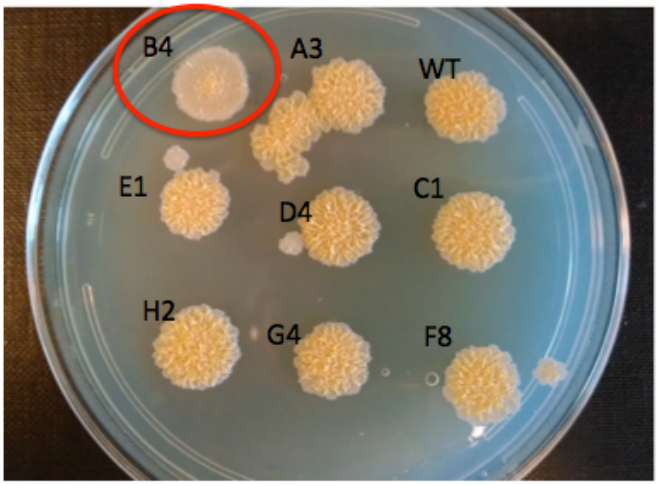

Figure 1B

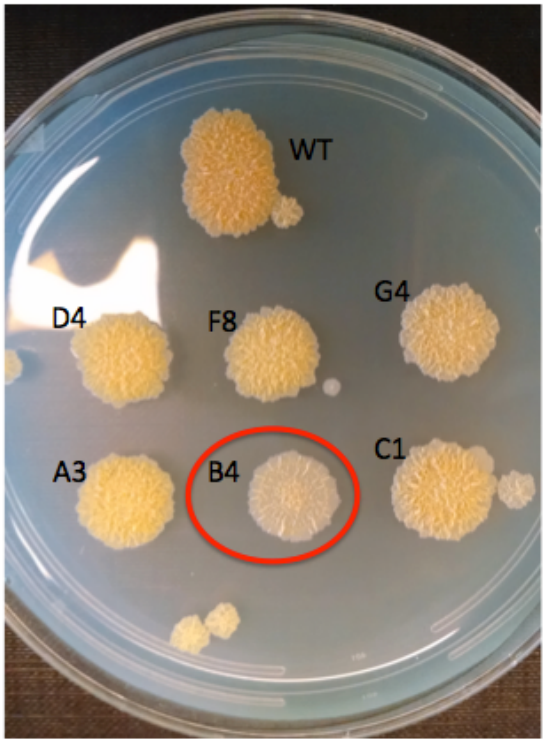

***Figures 1A and 1B*: The figures above show the 8 principal mutant colonies and the wild type (WT) grown on 7H11 agar. Note the unique morphology of B4.**

No significant difference in morphology between mutant colonies and wild type on swarming agar

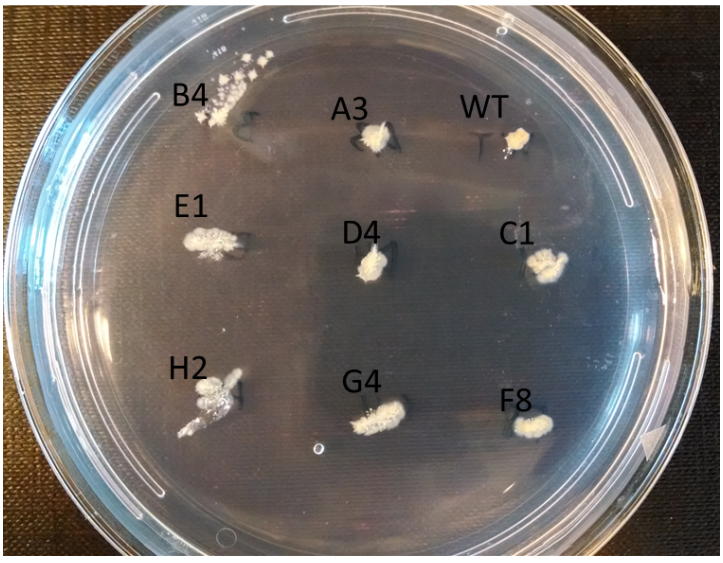

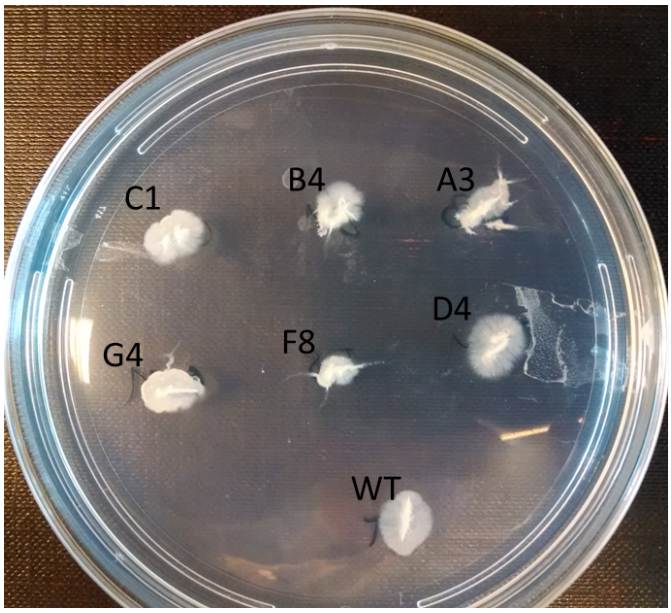

***Figures 2A and 2B*: The figures above show the 8 principal mutant colonies and the wild type (WT) grown on swarming agar. The appearance of B4 in Figure 2A is most likely a result of colonies growing on the surface, not a significant difference in morphology compared to the other mutants.**

No significant difference in growth rate between mutants and wild type

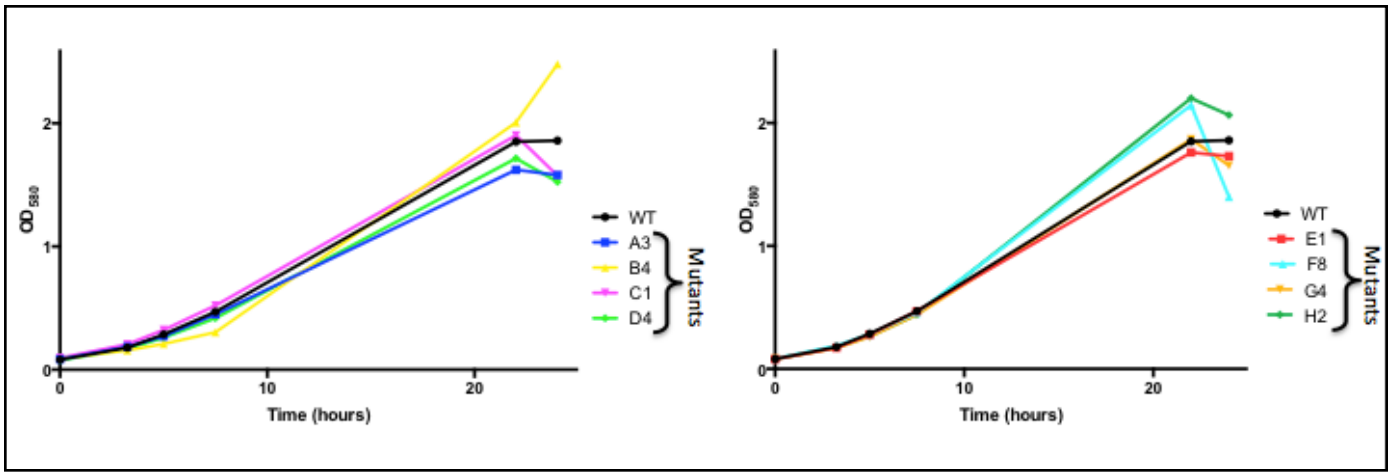

Figure 3: **The figure above shows the growth curves of the 8 principal mutants and the wild type (WT). All strains were grown up in liquid media with a starting OD580 of 0.1.**

All mutants showed increased resistance to Compound 1A, while Mutant D4 showed complete resistance

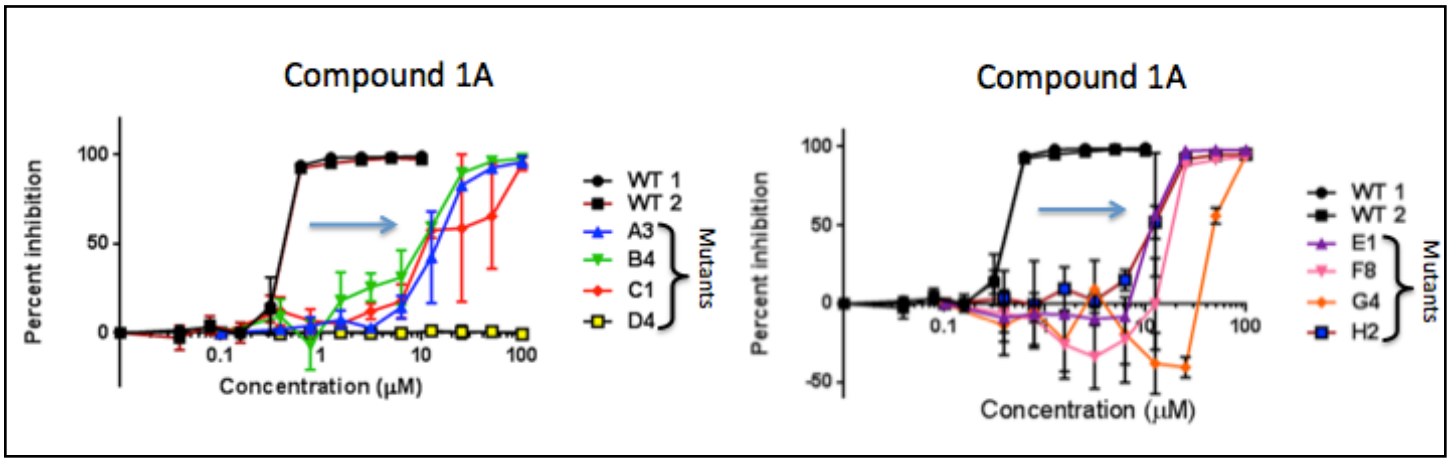

Figure 4: **The figure above shows the percent inhibition of the 8 principal mutant colonies and the wild type (repeated twice) when exposed to different concentrations of Compound 1A. Note the unique phenotype of D4, which shows complete resistance.**

Mutants and wild type had similar percent inhibition when exposed to ethambutol

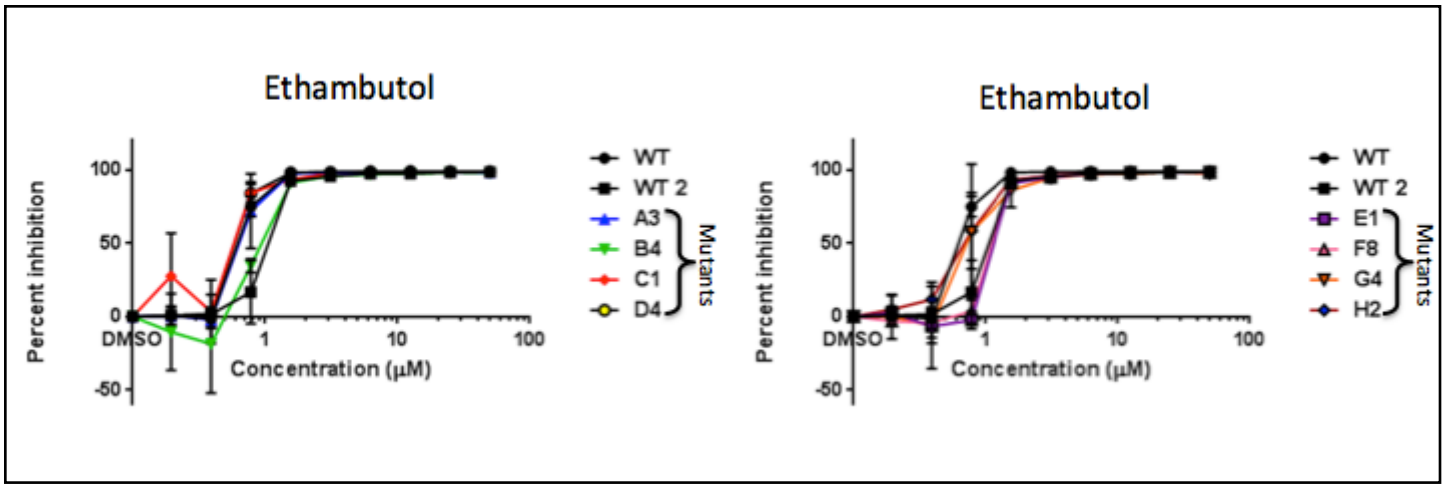

Figure 5: **The figure above shows the percent inhibition of the 8 principal mutant colonies and the wild type (repeated twice) when exposed to different concentrations of ethambutol. All mutant colonies show the same percent inhibition as the wild type, an expected result.**

Proline to Leucine Amino Acid change results in change in binding pocket

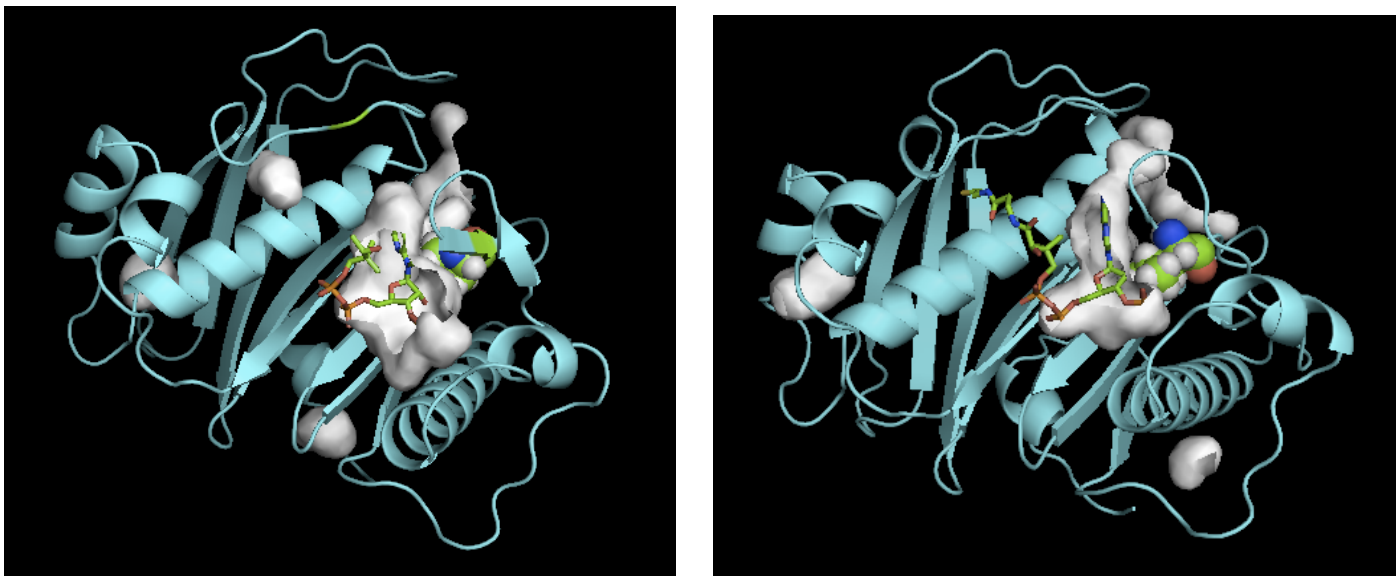

Figure 6: **The figure above shows the protein translated by Gene YMsm in its unmutated (left) and mutated (right) form. The mutant D4 had a nucleotide substitution in Gene YMsm that resulted in a proline to leucine amino acid change. Based on the figure, the mutation caused a change to the binding pocket, which may be the cause of resistance to Compound 1A. The figure was produced by I-TASSER14,15,16,17.**

References

1. Anderson, L., Dean, A., Falzon, D., et al. Global tuberculosis report 2015, 20th edition. Geneva: World Health Organization, 2015.

2. Spitters, C. E. (2012). Multidrug-Resistant Tuberculosis. In: Jong, E. C. and Stevens, D. L. eds. Netter's Infectious Diseases, Philadelphia: Elsevier Saunders, 2012: 544-553.

3. Gold, B., Pingle, M., Brickner, S. J., Shah, N., Roberts, J., Rundell, M., ... Nathan, C. F. (2012). Nonsteroidal anti-inflammatory drug sensitizes Mycobacterium tuberculosis to endogenous and exogenous antimicrobials. Proceedings of the National Academy of Sciences of the United States of America, 109(40), 16004–11.

3. Bryk, R., Gold, B., Venugopal, A. et al. (2008). Selective killing of Nonreplicating Mycobacteria. Cell Host & Microbe, 3(3), 137-145.

4. Nathan, C. and Barry III, C. (2015). TB drug development: immunology at the table. Immunol Rev., 264(1), 308-318.

5. Wallis, R., Maeurer, M., Mwaba, P. et al. (2016). Tuberculosis-advances in development of new drugs, treatment regimens, host-directed therapies, and biomarkers. Lancet Infect Dis., 16(4), e34-46.

6. Warrier, T., Martinez-Hoyos, M., Marin-Amieva, M. et al. (2015). Identification of novel Anti-mycobacterial compounds by screening a pharmaceutical small-molecule library against nonreplicating Mycobacterium tuberculosis. American Chemical Society Infectious Diseases, 1(12), 580-585.

7. Rebollo-Lopez, M.J., Lelievre, J., Alvarez-Gomez, D., et al. (2015). Release of 50 new, drug-like compounds and their computational target predictions for open source anti- tubercular drug discovery. PLoS ONE, 10(12): e0142293.

8. Martinez, A., Torello, S., and Kolter, R. (1999). Sliding motility in mycobacteria. Journal of Bacteriology, 181(23), 7331-7338.

9. Van Soolingen, D., Hermans, P., De Haas, P., Soll, D., and Van Embden, J. (1991). Occurrence and stability of insertion sequences in Mycobacterium tuberculosis complex strains: Evaluation of an insertion sequence-dependent DNA polymorphism as a tool in the epidemiology of tuberculosis. Journal of Clinical Microbiology, 29(11), 2578-2586.

10. Chester, N. and Marshak, D.R. (1993). Dimethyl sulfoxide-mediated primer Tm reduction: a method for analyzing the role of renaturation temperature in the polymerase chain reaction. Analytical Biochemistry, 209(2), 284-290.

11.Gutterson, N.I., and Koshland, D.E. Jr. (1983). Replacement and amplification of bacterial genes with sequences altered in vitro. Proc Natl Acad Sci USA, 80(16), 4894-8.

12. Lee, R., Hurdle, J., Liu, J., et al. (2014). Spectinamides: A New Class of Semisynthetic Anti-Tuberculosis Agents that Overcome Native Drug Efflux. Nat Med., 20(2), 152-158.

13. Yang, J., Yan, R., Roy, A., Xu, D., Poisson, J., and Zhang, Y. (2015). The I-TASSER Suite: Protein structure and function prediction. Nature Methods, 12(1), 7-8.

14. Yang, J. and Zhang, Y. (2015). I-TASSER server: new development for protein structure and function predictions. Nucleic Acids Research, 43(W1), W174-W181.

15. Yang, J. and Zhang, Y. (2015). I-TASSER server: new development for protein structure and function predictions. Nucleic Acids Research, 43(W1), W174-W181.

16. Roy, A., Kucukural, A., and Zhang, Y. (2010). I-TASSER: a unified platform for automated protein structure and function prediction. Nature Protocols, 5(4), 725-738.

17. Zhang, Y. (2008). I-TASSER server for protein 3D structure prediction. BMC Bioinformatics, 9: 40.

A novel approach to using pseudospecies effects exhibited by dsDNA waterborne bacteriophages as an indicator for mutagenic contamination

Phillip Kutcher

Annotated by Julian Rubinfien

Abstract

Bacteriophages (viruses that infect bacteria) are the most abundant biological entities on Earth. Deciphering their inner processes is therefore essential to acquiring knowledge of the predominant selective force acting on the biogeochemical cycles of our planet. One area in which research of bacteriophages is lacking is the quasispecies phenomenon, which is well documented for RNA and ssDNA viruses, but was never observed in dsDNA viruses. Pseudomonas phage phiNFS exhibits alternating cycles of pseudolysogeny and lysis. The objective of this project was to uncover the genetic reason for this eccentric growth pattern. Analysis of phiNFS samples with 6000x coverage of every base revealed 15 sites in the ~40 kb genome at which the base would undergo spontaneous single nucleotide polymorphism more than 1%, suggesting existence of a quasispecies phenomenon in the phiNFS population. One potential explanation for why polymorphism occurs is that the accumulation of mutations is driven by physiological changes and mutations in host bacteria as well as by error prone DNA polymerase encoded by this phage. This first result is incredible because it means that phiNFS and similar phages can be used as indicators for mutagenic compounds, as these compounds will affect the host bacteria and consequently the phages.

Introduction

Bacteriophages are the most abundant biological entities on Earth. Through lysis of their hosts, transduction processes, and as the predominant selective force acting on the bacterial domain, phages inherently influence the biogeochemical cycles which shape our planet.

Due to the intrinsic relationship that phages have with their hosts, changes in the host population are subsequently reflected in the phage population. Combined with the fact that viruses represent one of the greatest levels of genetic diversity on the planet, it is not surprising that studies into viral communities are becoming commonplace.

With rapid advances in sequencing technologies, the study of uncultured viral constituents in a variety of environments (known as viral metagenomics) has provided a great deal of information about the incredible diversity of this world.

Antagonistic coevolution between interacting species results in recurrent natural selection via constant cycles of adaptation and counter-adaptation, known as the Red Queen Hypothesis (Van Valen, 1973; 1974). Such interactions are at their most intense between bacteria and their phages. As bacteria evolve to be more resistant to phage attacks, phages must simultaneously adapt to be more and more deadly to bacteria, regardless of resistance. This is the reason that bacteriophages are one of the fastest mutating classes of organism on the planet. Studies of viral evolution thus provide an unparalleled insight into the truly remarkable elasticity of living entities.

'THIS IS A PULL QUOTE TO HELP THE READER STAY INTERESTED AND FOCUSED.'

Whilst studies of the effects of phage evolution in relation to changes in host range are abundant (Gomez & Buckling, 2011), as are those directed towards understanding the quasispecies phenomena exhibited by RNA and single strand DNA (ssDNA) viruses (Vignuzzi et al, 2006), studies examining the molecular processes at play in double strand DNA (dsDNA) representatives are found to be lacking.

This project aims to address the absence of research that concerns the operation of a quasispecies-like phenomenon occurring in phiKMVviruses, a subset of the larger group of T7Viruses. T7Viruses are notable for being the viral counterpart of bacterium Pseudomonas aeruginosa, a multidrug resistant pathogen, so called because of its natural antibiotic resistance.

More specifically, the project concerns itself with the operation of specific phiKMVvirus phiNFS, which exhibits a growth cycle of lysis and stasis. The sequencing of phiNFS revealed a 99% relatedness to bacteriophage phiKMV, for which such growth behaviors have not been reported. Thus, the project aims to discover why phiNFS, and only phiNFS, exhibits these eccentric growth behaviors.

This goal is important because the observation of a single phage's eccentric growth patterns can be a useful factor in determining other information about the phage, as well as being used as a factor to determine the effects of external factors on the phage and as an indicator of outside force action or inaction onto a target bacteriophage.

Materials and Methods

1) Water samples (5-20 litres) were collected from the River Lagan.

2) Bacteriophages were filtered out of the water samples, and phage DNA was isolated.

3) DNA libraries were prepared and sequenced on the Illumina MiSeq platform.

4) Reported sequences were aligned with a reference genome, and the differences, including single nucleotide polymorphisms, were identified and analyzed.

Results

My analysis revealed 15 Single Nucleotide Polymorphism (SNP) mutation sites (including 13 nonsynonymous ones), with each one having a single nucleotide change between the reported consensus of the reference phiNFS genome and the reads received from the samples. (Fig. I)

7 SNPs are in coding regions of the same protein, Putative Tail Fiber protein gp38, which is the major host tropism determinant (Wang et al, 2000). 2 of these SNPs lie within the same codon.

The rate of mutagenesis of these sites as a percentage of the entire sequence mass varied from 1.12% - 53.05% (Fig. I). Notable cases of single nucleotide polymorphisms include one at a fixed rate of 23.37 (g.5046T>G, resulting in E>A within the protein product) and another at a fixed rate of 33.52% (g.5064T>A, resulting in E>V within the protein product) (Fig. II). Interestingly, these two SNPs appear to interact with each other and assemble into several possible combinations, preferring some combinations of mutant-wild over others.

Out of the 1317 total occurrences of this base in the reads, 38.11% of the sequences contain both bases in their wild-type form, 23.96% of the reads contain only position 5046 mutated, and 37.42% contain only 5064 mutated. Only 0.51% of the total reads of these positions contain both positions mutated.

This is a citation. Citations and important notes can be placed on the same page they are referencing here at the bottom. *Author,* Publisher, 2014

Perhaps the most dimorphic example of all of the single nucleotide polymorphisms observed is the apparent linkage between two read positions that code for the same amino acid in the NAT-Acetyl Transferase protein; one with a fixed mutation rate of 46.41% (g.35224G>A, resulting in S>L within the protein product) and another with a fixed mutation rate of 53.05% (g.35225A>G, resulting in S>P within the protein product) (Fig. III).

The case for these two single nucleotide polymorphisms being linked can be brought by observing the mutation rate of the two positions in concert. Only 0.01% of the total matches had only position 35224 mutant and only 4.58% of the total matches has only position 35225 mutant; overwhelmingly, these two positions were either both mutant or both wild-type.

Discussion

In this work I discovered that in bacteriophage phiNFS's genome there are 15 polymorphic sites exhibiting significant variation (over 1% and up to 53.05%). Such a phenomenon has been previously studied in RNA and ssDNA viruses, but was never shown to exist in dsDNA phages. The existence of such variable sites in dsDNA phages needs explanation and further studies.

I also found that the number of phiNFS SNPs in liquid medium was three times the number of phiNFS SNPs grown on plates.

Theories to Explain Results

Given that some of the sites where polymorphism has been found are associated with phage adsorption, polymorphic sites in the key genes (responsible for the specificity) probably play an important role in the phage-host interactions. The reason why SNPs arise in phiNFS may be the error prone DNA polymerase encoded by the phage.

Conclusion

Over the course of the summer I spent under the guidance of my mentor, I worked with him to discover the intricacies of the eccentric and hitherto unexplainable growth patterns of a specific bacteriophage, phiNFS, trying to justify its curious alternating growth pattern of lysis and pseudolysogeny. We found a conclusion that was never before seen in the realm of dsDNA viruses, only ever being observed with RNA based phages. We also formulated a hypothesis about the prevalence of single nucleotide polymorphisms in liquid media by the physiological makeup of host bacteria.

Possible applications of this work in other fields (including ecology and nature conservation) are numerous, including the monitoring of waterborne pathogens in bodies of water.

Figures

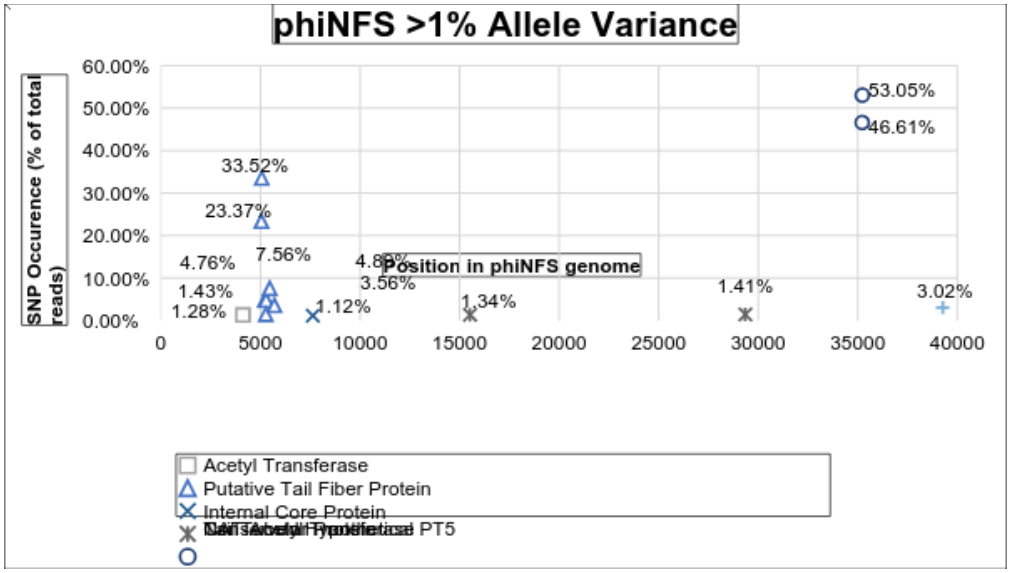

Figure I: Analysis of the 6000x coverage reads of the phiNFS genome revealed a total of 15 Single Nucleotide Polymorphism mutation sites with a genome deviance rating of >1%, with each site having a single nucleotide diversion between the normal phiNFS genome and the reads received from the samples show up in more than 1% of the total reads of that site. One of these sites was located on the promoter for the virus, and thus was discounted from results due to not coding for any specific protein. Seven of these SNPs are coding regions of the same protein, the Putative Tail Fiber protein, which is the major host tropism determinant. 2 pairs of these SNPs each lie within the same codon.

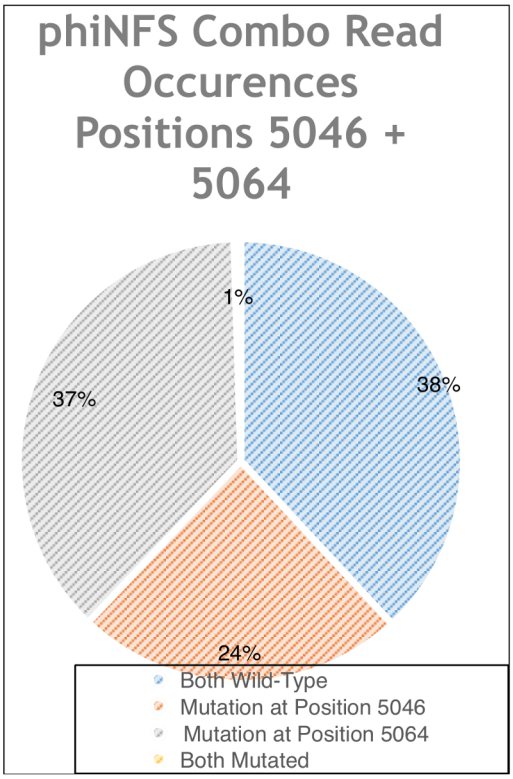

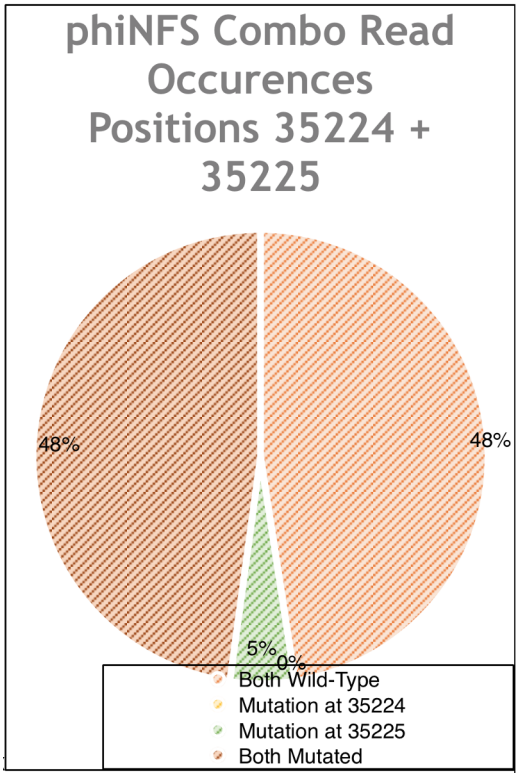

Figure II: Analysis of SNP occurrence rates for positions 5046 and 5064 of the phiNFS genome in concert with one another revealed a striking differentiation from expected results. In contrast to the expected ratio of about 25% occurrence of each combination of the two genes status of being mutant or wild-type, out of the 1317 total occurrences of this base in the reads, 38.11% of the reads contain both bases in their wild-type form, 23.96% of the reads contain only location 5046 mutated, and 37.42% contain only 5064 mutated. Only 0.51% of the total reads of these locations contain both locations mutated. This means that one combination of the two bases, that of both positions being mutated, was unfitting for the genome by a vast margin.

Figure III: Perhaps the most dimorphic example of all of the SNPs observed in the phiNFS genome is the apparent linkage between read locations 35224 and 35225. The case for these two single nucleotide polymorphisms being linked can be brought by observing the mutation rate of the two locations in concert. Of the 21,406 total matches to this section of the phiNFS genome, 47.84% of the reads contained both locations in their wild-type form, leaving the genetic sequence unchanged and the Leucine still being produced. However, 47.56% of the total matches to this section of the genome had both sites having undergone mutation, with the final amino acid resulting from not one but two of the amino acids in the codon being changed, being Phenylalanine. Only 0.01% of the total matches had only location 35224 mutant and only 4.58% of the total matches has only location 35225 mutant. Overwhelmingly, these two locations were either both mutant or both wild-type, which lends credence to the theory that they are linked.

References

1) Brennerova, M.V., Josefiova, J., Brenner, V., Pieper, D.H. and Junca, H., 2009. Metagenomics reveals diversity and abundance of meta-cleavage pathways in microbial communities from soil highly contaminated with jet fuel under air-sparging bioremediation. Environmental microbiology, 11(9), pp.2216-2227.

2) Gaufin, A.R. and Tarzwell, C.M., 1952. Aquatic invertebrates as indicators of stream pollution. Public Health Reports, 67(1), p.57.

3) Gomez, P. and Buckling, A., 2011. Bacteria-phage antagonistic coevolution in soil.

4) Science (New York, N.Y.), 332(6025), pp. 106-109.

5) Jin, H., Lin, C.T., Shang, J., Wilkins, M., Liu, Y., Gong, W., Xu, W., Squier, T. and Long, P., 2013. Aβ-Like Peptide Displayed on Bacteriophage T7 Catalyzes Chromate and Uranyl Reduction. Journal of Environmental Protection, 4, pp. 857-868.

6) Skvortsov, T., de Leeuwe, C., Quinn, J.P., McGrath, J.W., Allen, C.C., McElarney, Y., Watson, C., Arkhipova, K., Lavigne, R. and Kulakov, L.A., 2016. Metagenomic Characterisation of the Viral Community of Lough Neagh, the Largest Freshwater Lake in Ireland. PloS one, 11(2), pp. 0150361.

7) Suenaga, H., Ohnuki, T. and Miyazaki, K., 2007. Functional screening of a metagenomic library for genes involved in microbial degradation of aromatic compounds. Environmental microbiology, 9(9), pp.2289-2297.

8) Van Valen, L., 1973. A new evolutionary law. Evolutionary Theory, 1, pp. 1-30.

9) Van Valen, L., 1974. Molecular evolution as predicted by natural selection. Journal of Molecular Evolution, 3(2), pp. 89-101.

10) Vignuzzi, M., Stone, J.K., Arnold, J.J., Cameron, C.E. and Andino, R., 2006.

11) Quasispecies diversity determines pathogenesis through cooperative interactions in a viral population. Nature, 439(7074), pp. 344-348.

CEP-1, p53 Homologue, Modulates Fat Metabolism and Longevity

Nina Uzoigwe

Annotated by Alexandra Wen

Abstract

Although autophagy proteins and their use of lipids ensure quality control in metabolism, they are linked to aging and their loss is detrimental towards health and lifespan. However, lipid profiles of long-lived *Caenorhabditis elegans* suggest that lipids are beneficial towards lifespan and have been evolutionarily conserved. In this study, I sought to determine the role of autophagy genes associated with longevity, specifically the allele *gk138* in the gene *cep-1*. Results indicate that *cep-1* is not only a critical modulator of the lifespan of *C. elegans*, but the loss of function of *cep-1* and *atg-7* significantly increases the lipid droplet concentrations compared to wild-type animals.

Introduction

The consumption of the body's own tissue as a metabolic process occurring in starvation and certain diseases.

A transparent nematode.

The type that is found naturally. Is designated with "+".

Organelle in the cytoplasm of eukaryotic cells. Contains degradative enzymes enclosed in a membrane.

Double-membraned vesicles that contain cellular material that will be degraded by autophagy. A membrane forms near autophagic cargo and expands until it encloses it.

The breakdown of fats and other lipids by hydrolysis to release fatty acids. Also known as lipophagy.

An desaturase enzyme that removes two hydrogen atoms from a fatty acid, creating a carbon/carbon double bond. Convert saturated fatty acids to MUFAs.

TP53 or tumor protein. A gene that codes for a protein to regulate the cell cycle and suppresses tumors.

Enzymes that catalyze the first step in the ubiquitination reaction, which target a protein for degradation.

Autophagy is a pathway that maintains cellular homeostasis by degrading macromolecules and organelles in lysosomes in a process called macroautophagy. Lipids can also undergo degradation through the sequestration of autophagosomes and autophagy-related proteins, called ATGs, that fuse with lysosomes (3,5). This process, lipolysis, ensures control of metabolism and energy through the hydrolysis of triglycerides into free fatty acids. However, triglycerides have been linked to aging (Lapierre et al., 2011).

The lipids extracted from the offspring of the long-lived individuals contain a higher ratio of monounsaturated fatty acids (MUFAs) over polyunsaturated fatty acids (PUFAs) (4). These worms express increased levels of Δ9 enzymes. However, PUFAs are vulnerable to oxidation and promote aging, generating radical oxygen species (ROS).

In this study, I sought to further characterize the role of autophagy genes and their association with longevity. Both mammalian *p53* and its nematode homolog *cep-1* have been described as tonic inhibitors of autophagy (5). When deleted or inhibited, they have been known to regulate genotoxic stress to relieve metabolic stressors and organelle damage (6,7,8,9,10).

I decided to investigate the lipid droplet staining of *C. elegans* with this genotype to see the relationship between longevity and the induction of autophagy. I also conducted a lipid droplet staining of *C. elegans* with *atg-7(bp411)*, a mutation in *atg-7*, an autophagy gene that encodes an E1 that is essential for lipid homeostasis. Results show that *cep-1* is not only a critical modulator of the lifespan of *C. elegans*, but a loss of function in *cep-1(gk138)* resulted in a significant increase in lipid droplet concentrations when compared to the *atg-7(bp411)* and wild-type animals, showing that *cep-1* plays a crucial role in regulating lipid droplet metabolism.

Staging of C. elegans (Images from wormbook.org)

FIGURES SHOWN ON NEXT PAGE

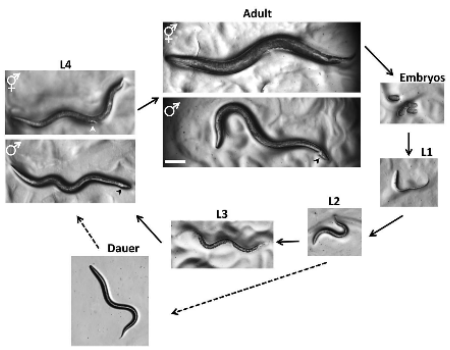

Figure 1.1: Staging of C. elegans.

As seen to the left, this is the developmental staging progression of *C. elegans*. L4 hermaphrodites were used for all staining of the lipid droplets, and their lipid concentration was stained by Oil-Red-O. Once the worms were stained, they were imaged with an Axiocam at 16x magnification. To measure the Oil Red-O Staining intensity, ImageJ was used.

Hermaphrodites in the fourth larval stage. Hermaphrodites and males sperm.

Results

Table 2.1 Oil Red-O Staining of Lipid Droplets (Representative Images of Each Strain)

N2 (wild type)			
atg-7			
cep-1	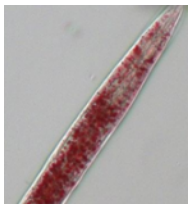		

Table 2.1 shows the Oil Red-O Staining of the lipid droplets of representatives from each of the strains. The animals with the allele *atg-7 (bp411)* have a visibly significant decrease in their lipid droplet concentrations in comparison to the presence of the droplets in the wild type.

Table 2.2: Relative Oil Red-O Intensity in cep-1, atg-7 and wild-type animals

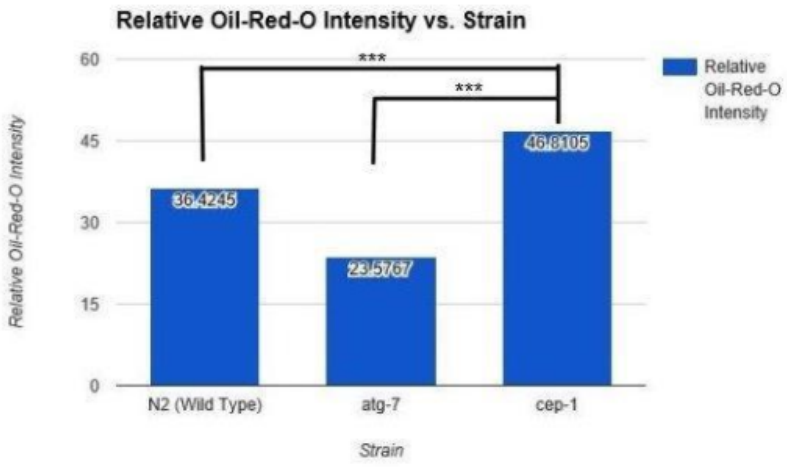

Quantification reveals that *cep-1(gk138)* mutants have high lipid droplet storage, whereas *atg-7(bp411)* mutants have a decrease in Oil-Red-O staining.

Table 2.2 shows the means of the Oil Red-O Intensities found from 3 trials of staining. As seen above, the animals with the *cep-1(gk138)* mutation statistically had the higher amount of lipid droplet staining when compared to those with *atg-7(bp411)* and N2. Mutants with *cep-1(gk138)* were significantly different from those of *atg-7(bp411)* and wild type.

Conclusions

Mammalian *p53* and its nematode homolog *cep-1* act as inhibitors of autophagy, which means that their deletion stimulates a continuous state of it (5). We found that *cep-1* mutants have an increase in lipids as determined by the staining, demonstrating a previously unknown interrelationship between autophagy and lipid metabolism in *cep-1(gk138)* mutants. In addition to the inhibition of *atg-7*, my results suggest that *cep-1* normally regulates lipid droplet content, and that *cep-1(gk138)* mutants either synthesize more triglycerides or breakdown less.

We hypothesize that there may be an apparent decrease in lipophagy in these long-lived worms, raising the question of whether or not increased lipid droplet levels also contribute to or result from the longevity found in these mutants (5). The next step would be to create a double mutant that consists of a loss of function in both *cep-1(gk138)* and *atg-7(bp411)* and stain them with Oil Red-O to check whether the loss of *cep-1* and *atg-7* activity would impact the concentration of lipid droplets. With this information, our knowledge of *p53* will be greatly enhanced. One can not only pinpoint what it does to impact longevity in C. elegans, but also what can be done to increase the lifespan of the human cell.

Acknowledgements

I would first like to recognize the PI (principal investigator) of the laboratory, Dr. Alicia Melendez, an Associate Professor of Biology. She helped me to go in the right direction in terms of ideas for my research. I would also like to recognize Melissa Silvestrini and Nicholas Palmisano, who are PhD students in the Meléndez lab, pursuing their own research. They helped me to familiarize myself with the lab environment and know how to carry out the procedures.

References

1. Gonzalez-Covarrubias, V. (2013) *Lipidomics in longevity and healthy aging. Biogerontology* 14, 663-672

2. Nektarios Tavernarakis, Angela Pasparaki, EzgiTasdemir, Maria Chiara Maiuri & Guido Kroemer (2008) *The effects of p53 on whole organism longevity are mediated by autophagy*, Autophagy, 4:7, 870-873, DOI: 10.4161/auto.6730

3. Ouimet M, et al. *Autophagy regulates cholesterol efflux from macrophage foam cells via lysosomal acid lipase*. Cell Metab, 2011; 13:655-667 [PubMed: 21641547]

4. Schroeder, E. A., & Brunet, A. (2015, November). Editorial Board and Contents. *CellPress: Trends in Endocrinology & Metabolism*, 26(11), 589-592. doi:10.1016/s1043-2760(15)00188-5

5. Singh R, et al. *Autophagy regulates lipid metabolism*. Nature, 2009; 458:1131-1135. [PubMed: 19339967]

6. Levine B., Kroemer G. *Autophagy in the pathogenesis of disease*. Cell 2008; 132:27-42

7. Klionsky, DJ. *Cell biology: regulated self-cannibalism*. Nature 2004; 431:31-2. 31.

8. Mizushima N, Levine B, Cuervo AM, Klionsky DJ. *Autophagy fights disease through cellular self-digestion*. Nature 2008; 451:1069-75.

9. Tasdemir E, Maiuri MC, Tajeddine N, Vitale I, Criollo A, Vicencio JM, Hickman JA, Geneste O, Kroemer G. *Cell cycle-dependent induction of autophagy, mitophagy and reticulophagy*. Cell Cycle 2007; 6:2263-7.

10. Vousden KH, Lane DP. *p53 in health and disease*. Nat Rev Mol Cell Biol 2007; 8:275-83.

Noninvasive detection of reactive oxygen species using xanthine/uric acid to use as a quantitative measure of tumors.

Yassmin Elbanna

Edited by Marie Ivantechenko

Abstract

An emerging body of data indicates that cancer cells have more **Reactive Oxygen Species,** which would theoretically aid in the imaging of tumors to see which parts are more active and understand how quickly the tumor is growing. In this context, reactive oxygen species are a key focus of the research into the chemical mechanisms underlying the progression of the disease. The goal to detect reactive oxygen species has motivated the construction of a primary detection. This project utilized Xanthine Oxidase, an enzyme that generates reactive oxygen species, to see how quickly the rate at which the Xanthine is picked up by the cell and is converted in the Uric Acid and other reactive oxygen species. To summarize, we believe that xanthine oxidase is the best method for measuring the rate at which Xanthine is picked up by a cell and converted into Xanthine oxidase. Using **ultraviolet visible spectroscopy**, we determined that Xanthine was the most efficient **metabolite** and that cells do in fact pick up the Xanthine and change in their absorbency. We then believe that this would a useful indication of the metabolic qualities of cancer. This project's importance is that this would develop a more efficient and detailed measurement of cancer imaging.

Chemically reactive species containing oxygen i.e. peroxides, superoxide, and hydroxyl radical

Measurement of the attenuation (reduction) of a beam of light after it passes through a sample or after reflection from a sample surface

Substance formed in or necessary for metabolism

Introduction

Magnetic resonance imaging is primarily a qualitative measure of tumors and the progression of cancer, yet it doesn't show the activity of these tumor cells. **Hyperpolarized Magnetic Resonance Imaging** is unique in that it allows for imaging of metabolites, overstepping the flaw held by Magnetic Resonance Imaging. This new technology is based on the premise that cancer cells use and metabolize nutrients differently and often at a faster rate, and it is unique in that it can be used to decide whether to continue treatment or to try a new approach [1].

There are fundamental differences between Hyperpolarized Magnetic Resonance Imaging and **radioactive contrast agents**, although both provide similar images. Hyperpolarized Magnetic Resonance Imaging contrast agents do not use ionizing radiation, making them a useful tool in analyzing the progression of cancer without endangering the patient and allowing for simultaneous imaging of multiple metabolites as well. This is a clear benefit because they enable measurements of metabolism as opposed to the tracer uptake typically measured with PET scans. The advantages of Hyperpolarized Magnetic Resonance Imaging include its increasing sensitivity due to the amount of nuclear spin polarization, its imaging of hyperpolarized contrast agents while in a low magnetic field, opening up new opportunities for **multi-modal imaging**, and its low-cost due to there no longer being a need for **high-field cryogenic magnets** [2].

Using hyperpolarization techniques, the signal from a given number of nuclear spins can be raised more than 100,000 times, enabling the imaging of nuclei other than proteins and their molecular distribution **in vivo** to be

Functional medical imaging technique for probing perfusion and metabolism using injected substrates

Substances used to enhance the visibility of internal structures in X-ray-based imaging techniques

Employs two or more imaging techniques in a single examination to allow acquisition of co-registered complementary data from tissue

Electromagnet made from coils of superconducting wire that must be cooled to cryogenic temperatures during operation

Performed or taking place in a living organism

visualized in a relatively small window of time, and the mapping of molecular distribution a few seconds after injection, offering a more direct form of molecular imaging.

Despite these differences, hyperpolarized contrast agents have a significantly shorter lifetime, anywhere from 0.5-5 minutes in vivo. This makes it slightly more difficult to take the image; however, it also offers an opportunity to perform repeat scans within minutes because there won't be any background signal [3].

Reactive Oxygen Species are byproducts of cellular metabolism produced during aerobic respiration in mitochondria (Figure 1) [4]. The superoxide produced during the aerobic respiration is converted to a second reactive oxygen species molecule, hydrogen peroxide, by superoxide dismutase. In the presence H2O2 ions, it can form hydroxyl radicals. These molecules can oxidize DNA, protein, and lipids, leading to negative effects and must be carefully controlled.

Cancer cells proliferate quickly in comparison to normal cells, and therefore require more energy to replicate DNA, resulting in more aerobic respiration, which in turn creates increased levels of reactive oxygen species, which have been observed during the replication of cancer cells [5]. These higher levels have been shown to inactivate tumor suppressors, such as phosphatase and tensin homolog (PTEN) [6]. Reactive oxygen species are a component of the killing response of immune cells to microbial invasion, ending up working to the benefits of cancers for multiple unintended reasons, specifically that reactive oxygen species interact with other things if there is too much DNA, leading to **genome instability** or the denature of proteins, furthering the progression of the cancer. An emerging body of data indicates that cancer cells have more reactive oxygen species, which would theoretically aid in the imaging of tumors to see which parts are more active and to understand how quickly the tumor is growing. In this context, reactive oxygen species are a key focus of the research into the chemical mechanisms underlying the progression of the disease.

Refers to a high frequency of mutations within the genome of a cellular lineage

Conclusions and Further Work

Our results demonstrated that Xanthine interacts best with superoxides in generating reactive oxygen species. These specific molecules would allow us to scavenge toxic species from cancer cells. This would generate a more effective metabolite imaging of **sarcomas** through hyperpolarized Magnetic Resonance Imaging, which would in turn be able to image the high concentrations of reactive oxygen species present within the cells.

Malignant tumor of connective or nonepithelial tissue

The project's implications can change the way cancer is assessed. By developing novel imaging probes for hyperpolarized Magnetic Resonance Imaging within cancer research, we can create a non-invasive, quantitative measure of tumors. This will increase our ability to provide more accurate prognoses and teach us more about cancer cells and their metabolic behavior.

References

1. More. (n.d.). Retrieved September 20, 2016, from https://www.mskcc.org/research-areas/labs/kayvan-keshari/overview

2. Peirce, B. A. (2016, September 8). Hyperpolarized MRI: A New Tool to Assess Treatment Response within. Retrieved September 20, 2016, from https://www.mskcc.org/blog/hyperpolarized-mri-new-tool-assess-treatment-response-within-days

3. Chekmenev, C. Y. (2013). MRI hyperpolarization and molecular imaging [PDF]. MI Gateway

4. Szeglin, B. (2016). Concurrent treatment of rapamycin and 15d-PGJ2 induces cancer cell death through a reactive oxygen species-dependent mechanism.

5. C. Gorrini, I. S. Harris, T. W. Mak, Modulation of oxidative stress as an anticancer strategy. Nature Reviews. 12, 931-947 (2013).

6. N. R. Leslie, D. Bennett, Y. E. Lindsay, H. Stewart, A. Gray, et al., Redox regulation of PI 3-kinase signaling via inactivation of PTEN. European Molecular Biology Organization. 22, 5501-5510 (2003).

7. Nessa, F., & Khan, S. A. (2014). Evaluation of antioxidant and xanthine oxidase inhibitory activity of different solvent extracts of leaves of Citrullus colocynthis.Pharmacognosy Research, 6(3), 218–226. http://doi.org/10.4103/0974-8490.132599

8. UV-Visible Spectroscopy. (n.d.). Retrieved September 20, 2016, from https://www2.chemistry.msu.edu/faculty/reusch/virttxtjml/spectrpy/uv-vis/spectrum.htm

9. Gowda, G. A. N., & Raftery, D. (2014). Quantitating Metabolites in Protein Precipitated Serum Using NMR Spectroscopy. Analytical Chemistry, 86(11), 5433–5440. http://doi.org/10.1021/ac5005103

10. THE ACTION OF HYDROGEN PEROXIDE UPON URIC ACID. SECOND PAPER ON HYDROGEN PEROXIDE AS A REAGENT IN THE PURIN GROUP. C. S. Venable Journal of the American Chemical Society 1918 40 (7), 1099-1120DOI: 10.1021/ja02240a014

Crowding Vision

Claire Jin

Annotated by Bhavin Tanna

Abstract

The fovea is the centermost part of the retina, the area is responsible for our central, detailed vision. Crowding is the difficulty of perceiving an object surrounded by clutter. Foveal crowding can impact daily activities that involve identifying small objects in a cluttered background. It's prominent in patients with amblyopia and may predict the slowness of reading of children with developmental dyslexia. Labs and clinics do not yet have the ability to measure foveal crowding. A new test is available to test it, however, involving identifying a digit.

Also known as a lazy eye; Decreased eyesight as a result of lacking visual development, usually developing early on in a person's lifetime.

A learning disability where the person with the disability generally has poor reading and spelling skills.

The minimum center-to-center spacing needed between certain objects so they can be recognized

Introduction

Crowding greatly limits visual perception. Due to crowding, a simple object, like a number, can only be recognized if clutter is a certain critical spacing away (Bouma, 1970; Levi, 2008; Pelli & Tillman, 2008).

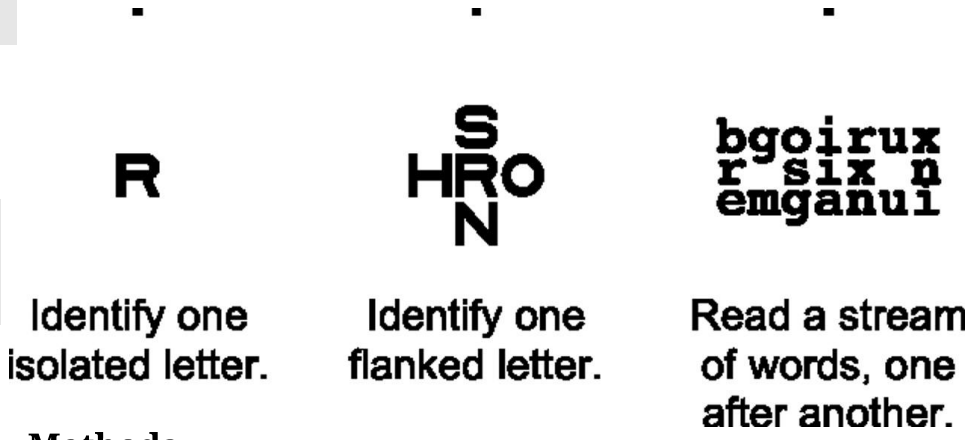

Flanked refers to side. Only one word appeals in the 3rd picture as a test.

Methods

We utilized a new acuity test called Critical Spacing.m on the program MATLAB 2015b with Psychtoolbox 3.0.12 extensions on computers running OS X or Windows. There are 9 custom designed letters, in "Sloan" and "Pelli" fonts, which are used with flankers. The observer's objective is to fixate at the cross hairs and identify it with flankers present. The letters only flash for a fraction of a second before they disappear. Correct answers are addressed with a "ding" sound. The acuity test measures the level of peripheral vision the observer has. The healthy level of critical spacing in the fovea is .05 degrees, but is higher in patients with amblyopia.

Vision around the area of attention/focus.

We needed a font that had a small width of the critical spacing we aimed to measure. The "Pelli" font has a 1:5 aspect ratio while the "Sloan" font has a 1:1 aspect ratio.

The Pelli and Sloan fonts respectively, with their height to width ratios as well as width to stroke ratios. Fonts have a small fraction of .05 deg critical spacing.

Results

CONDITION 1 **********

Spacing(deg)	P fit	P	Trials
0.115	0.10	0.00	1
0.201	0.10	1.00	1
0.244	0.11	0.00	1
0.674	0.25	0.00	1
0.875	0.39	0.00	1
0.933	0.43	0.00	1
0.961	0.46	1.00	1
0.990	0.48	1.00	2
1.004	0.50	1.00	1
1.019	0.51	1.00	1
1.062	0.55	1.00	1
1.105	0.58	0.50	2
1.148	0.62	1.00	1
1.220	0.68	1.00	2
1.306	0.75	1.00	1
1.794	0.96	1.00	2

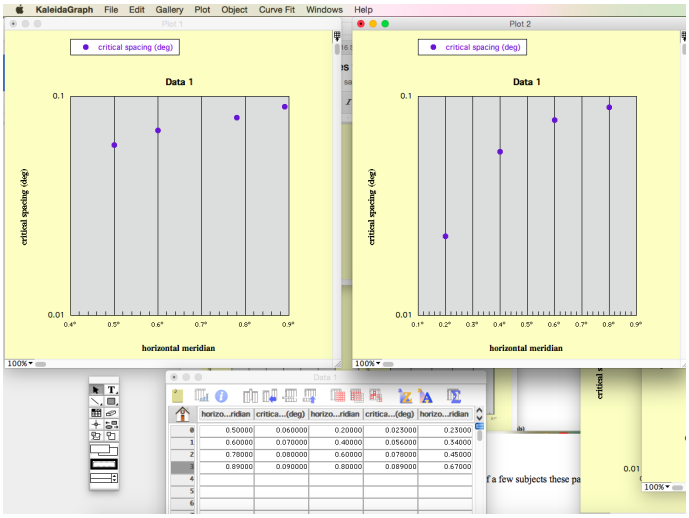

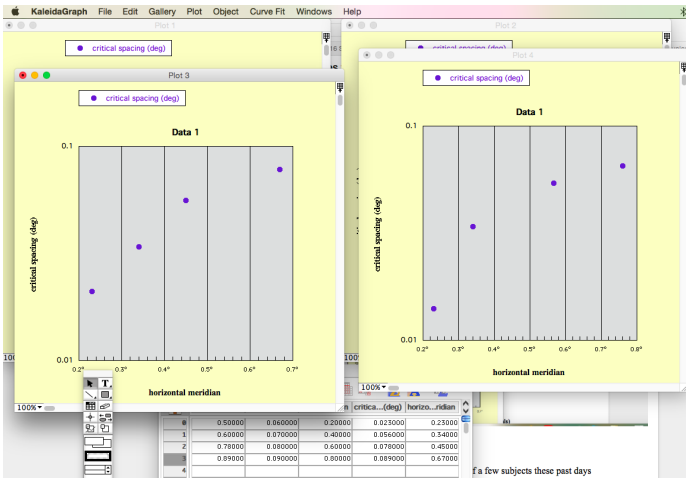

We uploaded data that we collected from two subjects into the KaleidaGraph and it output the polar graphs shown above.

Discussion

Foveal crowding limits visual perception and more severe cases of foveal crowding are present in patients with amblyopia. Unlike visual acuity, crowding is measured in critical spacing. The two are independent of one another. However, it is still unknown what accounts for crowding. One study conducted shows that the difference in accuracy between spaced and condensed stimuli was significantly associated with lower grey matter volume in the right collateral sulcus (Yong). This raises the possibility of crowding being associated with neuronal density.

A two-dimensional coordinate plane where each point that is plotted is determined by a distance from a given point and an angle from a given direction.

The darker tissue in the brain and spinal cord, which mainly consists of nerve cell bodies and dendrites (extensions of nerve cells that receive impulses and pass on/transmit synapses, which are signals that travel through nerve cells that release neurotransmitters, which enable transfer).

References

1. Yong, K. X., Shakespeare, T. J., Cash, D., Henley, S. M., Nicholas, J. M., Ridgway, G. R., ... & Schott, J. M. (2014). Prominent effects and neural correlates of visual crowding in a neurodegenerative disease population. Brain, 137(12), 3284-3299.

2. Bouma, H. (1970). Interaction effects in parafoveal letter recognition. Nature, 226, 177-178.

3. Levi, D. M. (2008). Crowding—An essential bottleneck for object recognition: A mini-review. Vision research, 48(5), 635-654.

4. Pelli, D. G., Tillman, K. A., Freeman, J., Su, M., Berger, T. D., & Majaj, N. J. (2007). Crowding and eccentricity determine reading rate. Journal of vision, 7(2), 20-20.

5. Song, S., Levi, D. M., & Pelli, D. G. (2014). A double dissociation of the acuity and crowding limits to letter identification, and the promise of improved visual screening. Journal of Vision, 14(5), 3-3.

6. Lev, M., Yehezkel, O., & Polat, U. (2014). Uncovering foveal crowding?. Scientific reports, 4, 4067.

7. Hariharan, S., Levi, D. M., & Klein, S. A. (2005). "Crowding" in normal and amblyopic vision assessed with Gaussian and Gabor C's. Vision research, 45(5), 617-633.

8. Huurneman, B., Boonstra, F. N., Cox, R. F., Cillessen, A. H., & van Rens, G. (2012). A systematic review on 'foveal crowding' in visually impaired children and perceptual learning as a method to reduce crowding. BMC ophthalmology, 12(1), 1.

9. Norgett, Y., & Siderov, J. (2014). Foveal crowding differs in children and adults. Journal of vision, 14(12), 23-23.

10. http://kellogg.umich.edu/theeyeshaveit/non-trauma/amblyopia.html

Identification of a Factor that Induces Prostate Specific Membrane Antigen (PSMA) Expression in Human Endothelial Cells

Judy Liu

Abstract

Prostate-specific membrane antigen (PSMA) is the most well-established, highly restricted cell surface prostate antigen. In addition to prostate cancer, PSMA is expressed in many other solid tumors. Importantly, PSMA expression is not found in adjacent normal endothelium, suggesting that a tumor-related factor may induce PSMA expression in neovessels. PSMA has become increasingly appealing to scientists as more research is conducted, specifically on its role in angiogenesis. Although it is now known that PSMA regulates angiogenesis, the specific factor(s) that induced PSMA expression in human umbilical vein endothelial cells (HUVEC) remains unknown. These previous studies paved the way for us to generate a monoclonal antibody that can block PSMA induction and use it to isolate the molecule that is responsible for the induction of PSMA expression in HUVECs. Clone 215 was produced using fraction 10 to 50 kDa from a kidney cancer cell line SK-RC-13. PSMA induction can be blocked by using clone 215 incubated with the conditioned medium from SK-RC-13 and MDA-MB-231. ELISA results showed that clone 215 binds to cancer secreted factor with molecular weight range 10 to 50 kDa. These results indicated that clone 215 binds the factor is the response for PSMA induction. We can use the monoclonal antibody from clone 215 to isolate and identify the factor that can induce PSMA expression in human endothelial cells. It will further expand our understanding in the role PSMA plays in tumor angiogenesis.

The PSMA gene is not commonly deleted in prostate cancer.

This substance lines the inside of blood vessels and lymphatic vessels.

This development of new blood vessels.

A plate-based assay technique designed for detecting and quantifying substances such as peptides, proteins, antibodies and hormones.

Antibodies that are made by identical immune cells that are all clones of a unique parent cell.

Introduction

Prostate-specific membrane antigen, commonly referred to as PSMA, is a 100 kilodalton (kDa) type 2 integral membrane glycoprotein. It is mainly expressed in prostate epithelial cells. Its expression is increased in prostate cancer, and 95% of prostate cancers are PSMA positive (1). J591 is a monoclonal antibody that binds to the extracellular domain of PSMA. It has been extensively studied in both preclinical models and clinical trials. J591 showed high-affinity binding to viable PSMA-expressing prostate cancer cell line LNCaP cells in the tissue culture and was rapidly internalized (2,3). This ability to be engulfed by the prostate cancer cells allows the bound antibody to deliver any contents attached to that antibody, such as immunotoxins, drugs, and radioisotopes, into the prostate cancer cells, which can then be utilized to fight and kill the cancer cells. Radiolabeled J591 has successfully targeted the metastatic tumor sites of prostate cancer. These studies have demonstrated that PSMA is an ideal candidate for antibody targeting therapy for prostate cancer.

Any of a class of proteins that have carbohydrate groups attached to the polypeptide chain.

Recently, scientists have established a model system to study PSMA expression in human umbilical vein endothelial cells (HUVEC). In their publication (entry), the data showed that they were able to induce PSMA expression in HUVEC cultured on Matrigel using conditioned medium from a subset of human cancer cell lines in both levels of mRNA and

A gelatinous protein mixture.

protein. The data also indicated that J591 was internalized by HUVEC with induced PSMA. Furthermore, the scientists were able to induce PSMA expression in HUVEC co-implanted with a kidney cancer cell line (SK-RC-13) in the mouse model. While these results suggest that cancer cells and HUVEC crosstalk induces PSMA expression, they did not address what is responsible for inducing PSMA expression in HUVEC. That is the gap we aim to fill in our project.

In this report, we used the in vitro model system from the study mentioned above to study PSMA expression and identify the factor that can induce PSMA expression in HUVEC. We generated a monoclonal antibody by using fractionated conditioned medium from SK-RC-13 to immunize the mice. This monoclonal antibody was able to block PSMA induction in HUVEC from conditioned medium. Figure 1 depicts the following: A. Tumor cells secrete factor(s) into the medium. Once released into the medium, the factor then cross-talks with HUVEC and transmits a signal that induces PSMA expression. B. In order to identify the factor (s), we decided to generate monoclonal antibody(s) that bind to the factor(s), which would therefore block PSMA induction. C. Isolation of the factor(s) by immunoprecipitation with monoclonal antibody(s) and identification of the factor(s) by mass spectrometry to determine the amino acid sequence. Succeeding to identify the factor(s) would contribute a great deal to the understanding of the role of PSMA in tumor angiogenesis.

The technique of precipitating a protein antigen out of solution using an antibody that specifically binds to that particular protein

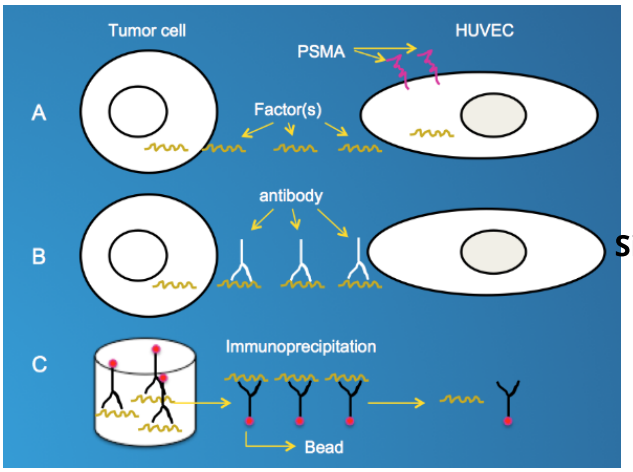

Figure 1.

A. Tumor cell secretes the factor(s) into the medium. The factor then cross-talks with HUVEC and transmit a signal that induces PSMA expression.

B. Tumor cell secretes the factor into the medium. A generated antibody then binds to the molecule, preventing cross-talk with HUVEC, which blocks PSMA expression.

C. Isolation of the factor by binding it with the monoclonal antibody and immunoprecipitation with protein G beads.

Materials and Methods

1) Cell cultures

2) Preparation and fractionation of conditioned medium

3) PSMA induction in HUVEC

4) Immunofluorescence staining

5) Generation of monoclonal antibodies

6) Screening of hybridoma clones by blocking induction of PSMA expression in HUVEC

7) Enzyme-linked mmunosorbent assay (ELISA)

A technique used for light microscopy with a fluorescence microscope and is used primarily on microbiological samples

Hybridomas are produced by injecting a specific antigen into a mouse, collecting an antibody-producing cell from the mouse's spleen, and fusing it with a tumor cell called a myeloma cell.

Results

To narrow the molecular weight range of the factor for the immunizations, the conditioned medium (SK-RC-13) was separated into three different fractions by using 50 kDa and 10 kDa filters. Fractions above 50 kDa, 50 to 10 kDa, and below 10 kDa were tested for the ability to induce PSMA expression in HUVEC and the unfractionated conditioned medium was used as the positive control for induction of PSMA expression. The results showed that of the three fractions, only the fraction 10 to 50 kDa highly induced PSMA expression. The unfractionated conditioned medium also strongly induced PSMA expression (Figure 2).

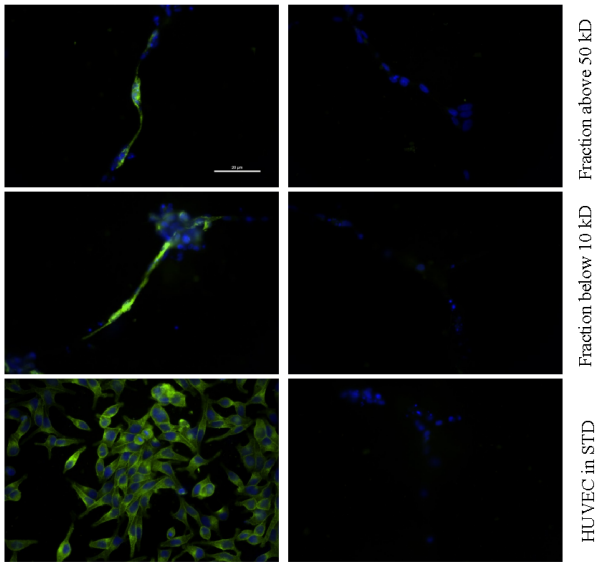

Figure 2. Determining the fraction for immunizations from SK-RC-13. Unfractionated conditioned medium (CM), fractions above 50 kD, 50-10 kD, and below 10 kD, were tested for the ability to induce PSMA expression in HUVEC. Fraction 10-50 kD showed strong fluorescence intensity. Fractions above 50 kD and below 10 kD showed very weak fluorescence intensity**.** Unfractionated CM also showed strong fluorescence intensity.

Screening of hybridoma clones

846 clones were picked from the fusion by a scientist for us to test the ability of each clone to block the induction of PSMA expression in HUVEC. Clone 215 that showed strong blocking of induction of PSMA expression in HUVEC and positive staining of SK-RC-13 was selected for further study. Clone 547, which showed a positive staining of SK-RC-13, but did not block PSMA expression in HUVEC, was used as the experimental control.

Discussion

PSMA is the most well-established, highly restricted cell surface prostate antigen. Beyond prostate cancer, PSMA expression is found in the tumor endothelium of a wide variety of solid tumors including renal cell carcinoma, breast carcinoma, colorectal, gastric adenocarcinoma, gynecological and head and neck cancers and glioblastoma, etc. [5–8]. Importantly, PSMA is not expressed in adjacent normal endothelium in these cancers, which suggest that tumor-related factors may induce PSMA expression in neovessels. A few studies were conducted in exploring the role of PSMA in tumor angiogenesis because absence of in vitro or in vivo experimental models of PSMA-expressing neo-vasculature. In this report, we used the in vitro endothelial model system that was developed by the scientists in the lab to study the regulation of PSMA expression in human endothelial cells. Our study was focused on identification of the factors that can induce PSMA expression in HUVEC. According to previous reports from the scientists in the lab, conditioned medium from 14 out of 19 human cancer cell lines were able to induce PSMA expression, which strongly suggested that the factor(s) was secreted into cultured medium by cancer cells. We should be able to collect and semi-purify it, and use it for immunizations. One of the advantages for using monoclonal antibodies to fish out the factor is the specificity of the monoclonal antibody, and another advantage is the functional assay in which induction of PSMA can be blocked by the monoclonal antibodies. For the reasons stated above, we generated monoclonal antibodies to bind to the molecules in the conditioned medium, and looked for the antibodies with blocking activity.

Conclusion and Further Study

In conclusion, in this report, our data demonstrated that we have generated a monoclonal antibody, and this monoclonal antibody was able to block the induction of PSMA expression in HUVEC from conditioned medium. This monoclonal antibody provides a valuable tool to isolate and identify the factor that is response for PSMA induction in human endothelial cells. It will help to understand the role of PSMA in tumor angiogenesis.

Clone 215 needs to be subcloned three times to make a stable clone. More supernatant and purified antibodies will be obtained after subcloning three times. We have limited supply of the supernatant from clone 215, preventing some key experiments from being done. In the future, a western blot should be performed against fraction 10 to 50 kDa and cell lysates from several cancer cell lines in order to determine the molecular weight of the factor.

Denoting the liquid lying above a solid residue after crystallization, precipitation, centrifugation, or other process

Computational Analysis and Prediction of Post-Stroke Recovery from Baseline Brain Connectome Metrics

Kimberly Ho

Annotatated by Benedict Ho

Abstract

Stroke is the fifth leading cause of death in the United States. It is the result of problems with blood supply to the brain. Stroke victims suffer motor, cognitive, and speech disabilities. There are various methods of rehabilitation, but it is not well known who will recover and to what extent. My research aims to help improve the accuracy of prognoses after stroke, and possibly to choose the most effective treatments.

Machine-learning techniques called neural networks are designed to simulate a biological neural system. The goal of the Artificial Neural Network (ANN) is to predict output variables based on input data. ANNs can predict how a patient is expected to recover based on measures extracted from their imaging. The results of this research shows promising benefits.

A prognosis is a prediction of the outcome of a disease.

Introduction

A stroke occurs when there is a blockage in the arteries that carry oxygen and nutrients to the brain.[26] The region of the brain that the blood flow cannot reach will lead to motor, language and cognitive impairments. Many stroke victims participate in rehabilitation to help regain some of the disabled functions. For example, a patient might practice walking with a cane to strengthen motor skills and muscles in the quadriceps. However, research in the specific areas of stroke recovery is limited. This research aims to explore the brain and its diseases and to answer: how can technology be an application in stroke recovery?

A dMRI measures water diffusion within the brain, which can provide information about the location and orientation of white matter tracts. A process called tractography uses dMRI information to trace likely white matter pathways.

The brain's structural connectome[39] is a map of all the major neural pathways in the brain.[33] Current research relies on diffusion magnetic resonance imaging (dMRI) to assess the brain. Once the pathways are traced, structural connectomes can be created. Structural connectomes represent the amount of white matter traced between pairs of gray matter regions via tractography.

The structural conncetome are descriptions of the connectivity network in the brain.

A network is used to summarize the structural connectome. The patient's imaging and other measures are entered into the artificial neural network (ANN) so the network can generate its own predicted post-stroke datasets. This technique has the ability to decipher patterns between datasets and explain the wiring of brain.

Materials and Methods

I. Subjects and Data

The National Institute of Health Stroke Scale (NIHSS) is a comprehensive neurological scale that provides a numerical measure of the patient's behavior and performance post-stroke. Physicians who observe the patient determine the measure. A higher NIHSS score indicates a more severe stroke. The accuracy of the measure depends on the observer's precise assessment.

This research utilizes public datasets of 16 anonymous post-stroke patients, consisting of magnetic resonance imaging (MRI) and functional MRI values between 86 different brain regions. In this research, MATLAB model R2013a and the Neural Network Fitting Tool were used. The input datasets represent the amount of structural connectivity between the 86 regions in the brain to each of the other regions. The total number of structural connections in the brain is 86 x 86, thus 7396 values. The output datasets represent the NIHSS section scores for each of the 16 patients.

The inputs and outputs are dsplayed on the following

Output Datasets
output1: 13 x 16 matrix; 13 NIHSS measurements of function at *baseline* after stroke for the 16 patients
output2: 13 x 16 matrix; 13 NIHSS measurement of function at *6-months follow-up* for the 16 patients

Input Datasets
input1: 7396 x 16 matrix; structural connectivity between 86 regions of the brain measured at *baseline* for the 16 patients
input2: 7396 x 16 matrix; structural connectivity between 86 regions of the brain measured at *6-months follow-up* for the 16 patients

II. Training Algorithms and the Neural Network Fitting Tool

The neural network simulates brain activity and is tested for its ability to predict stroke recovery. The neural network used in this research is a multi-layer ANN, which has several levels called hidden layers[37]. The Neural Network Fitting Tool creates an optimized model, but is sensitive to outliers.

Refer to diagram below.

Figure 1. Diagram of a Multilayer Neural Network. A multilayer neural network is a feed-forward model that maps input datasets onto output datasets using backpropagation techniques. This research utilizes multilayer neural networks. [A] The input layer consists of passive data that will not change when the model is training. [B] The hidden and output layers are active nodes that modify data in this structure. [Image from "Stock Market Prediction Using Neuroph Neural Networks." Copyright 2016 by Technobium.]

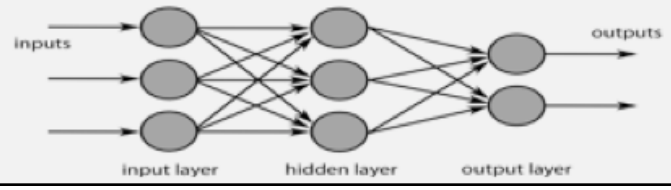

The forward phase of backpropagation computes the output value for each neuron based on weights from previous iteration. The next phase is the backward phase. This is the reverse of the forward phase. Weights at the current level would be updated before weights at the previous iteration. This computation allows the network to use error for neurons at the current level to estimate the error for neurons at the previous iteration.[30]

Backpropagation is a technique used to optimize weights of hidden neurons to accurately map inputs onto outputs. This technique assesses the error without knowledge of the output values.

The accuracy of the ANN's prediction is understood with regression analysis.[35] In Equation 1, a linear regression finds the best-fit line for a dataset, which is assessed using a statistic called R2.

Equation 1. Equation for R^2 Value. [A] A smaller sample size has a bigger impact on the regression. Because ANNs are sensitive to outliers, the regression can be greatly impacted when there is an outlier in a small sample. [B] p represents the hidden neurons in this research. [C] A R^2 value of 0 indicates that the model has no predictive value and a R^2 of 1 indicates that the model has perfect predictive value.

$$R^2 = 1 - \frac{(1 - R^2)(N - 1)}{N - p - 1}$$

R^2 = sample R-square *p = number of predictors* *N = total sample size*

The Neural Network Fitting Tool also uses mean square error (MSE) to evaluate error.

Equation 1. Equation for calculating Mean Square Error (MSE). [A] If the target and output datasets are closely related, error is close to 0.

$$E_{total} = \Sigma \frac{1}{2} (target - output)^2$$

target = the dataset provided by the user *output = model's predicted dataset*

ALL FIGURES ARE SHOWN ON THE FOLLOWING PAGES.

I. Relationship Between Training for Baseline Connectome and Baseline Function

It was hypothesized that because the signs of post-stroke in the first stage are easily visible, the measures determined by the NIHSS would match closely to results in the structural connectome.

This hypothesis was consistent with the results after training the model. The training for this relationship shows moderate error and a R2 of 0.8726. In Figure 4, the MSE of the majority of the samples lie near 0.1998.

In Figure 5, the regression for training, validation, and testing all show a regression close to 1. As the NIHSS measure increases, there are weaker connections, which demonstrates that this machine-learning technique is a faster and more convenient approach to measure the severity of the stroke.

II. Relationship Between Training for Baseline Connectome and 6-Months Follow-up Function

It is important to compare baseline connectivity to 6-months follow-up measures using ANNs to test how accurate the model's predictions are. In Figure 6, MSE values are lower in comparison to the training for baseline connectivity and baseline functions.

While there were at least two outliers, most of the error of the data trained resided at -0.083. This low MSE indicates the predictability power of neural networks. The decrease in MSE is a favorable indicator that the use of ANNs can be beneficial in this area. There is also a similar R2 0.863261, which is displayed in Figure 7. This value indicates the network predicted outcomes that were almost exactly the same as the target outputs.

III. Relationship Between Training for 6-Months Follow-up

In six months, the patient has improved, meaning the NIHSS will not be as accurate an indicator in the later stages of recovery.

As seen in Figure 9, the R2 is a low value of 0.15521. The test set resulted in a low R2 value because of the great error in this trial. As a result, the model's predicted output was not closely related to the data from the NIHSS.

Figure 5. Regression Plot for the Relationship: Baseline Connectivity and Baseline Functions. The R^2 is 0.872645. A value closer to 1 indicates that the predicted outputs are closely related to the actual targets. [A] The regression of the training set is 0.99953. From the analysis of the MSE, it can be concluded that the network predicted outputs closely related to the targets. This value proves that the network was able to predict an accurate set of outputs with respect to the target dataset. [Plots from MATLAB Neural Network Fitting Tool.]

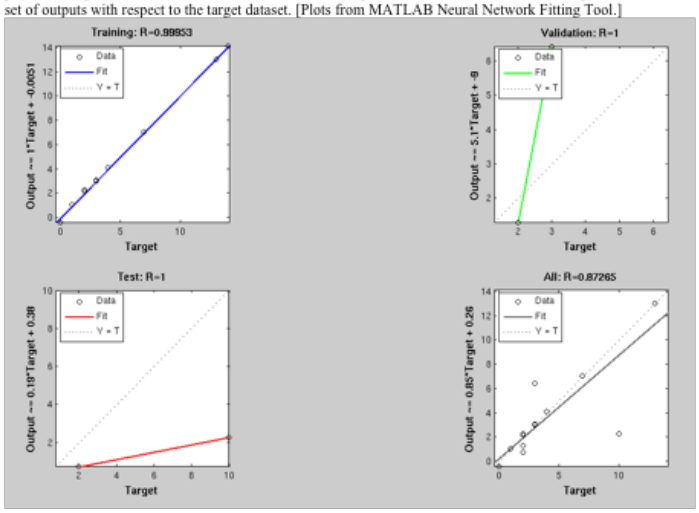

Figure 6. Error Histogram for the Relationship: Baseline Connectivity and 6-Months Follow-Up Functions. The MSE is 1.45685. [A] The diagram shows that most of the samples from training lie near an error of -0.083. [B] The error performance of the validation set is at one of the extreme ends. This indicates that the network may have failed to tune the optimal weights to predict outputs. [Histogram from MATLAB Neural Network Fitting Tool.]

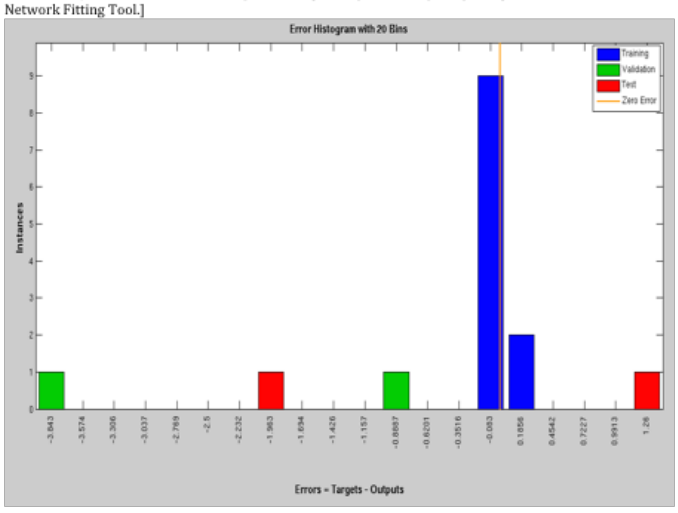

Figure 7. Regression Plot for the Relationship: Baseline Connectivity and 6-Months Follow-Up Function. The R^2 is 0.863261. [A] The regression of the training set indicates that the neural network determined a fit optimal set of weights to tune the parameters of the model. [B] The validation set failed to draw any relationship, as supported by Figure 6. [C] However, the overall regression shows a promising benefit of this technology. The network is a valuable tool because it can develop accurate prognoses for stroke recovery. [Plots from MATLAB Neural Network Fitting Tool.]

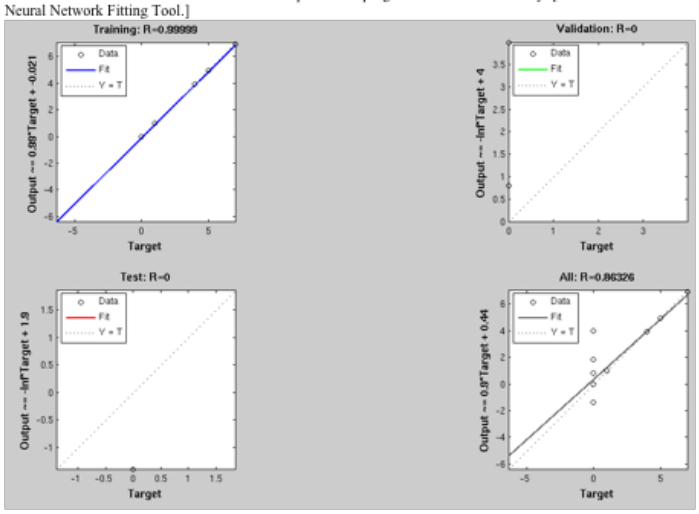

Figure 8. Error Histogram for the Relationship: 6-Months Follow-Up Connectivity and 6-Months Follow-Up Functions. [A] The diagram shows instances where error is scattered and not centered near 0. This suggests that the model did not predict favorable results. [B] The high MSE values indicate that the parameters of the network were not fit to create an output dataset that matches the target dataset. There may be inconsistencies regarding the NIHSS evaluation taken 6-months post-stroke. In addition, the network was not informed of any important patient history that can drastically affect datasets. [Histogram from MATLAB Neural Network Fitting Tool.]

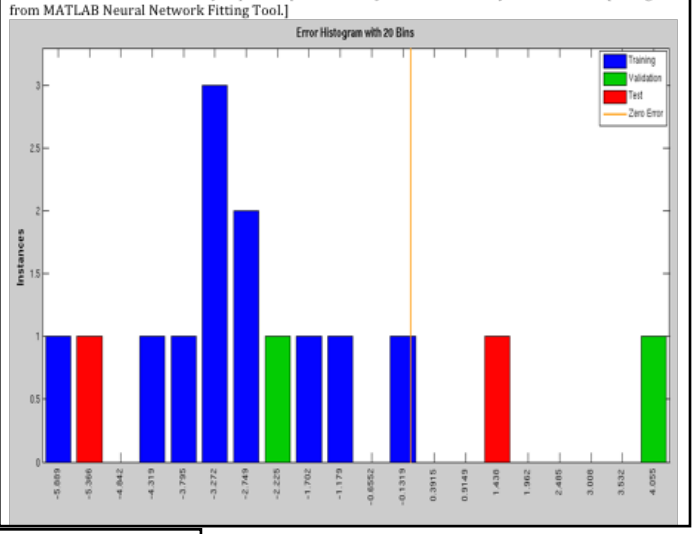

Figure 9. Regression Plot for the Relationship: 6-Months Follow-Up Connectivity and 6-Months Follow-Up Functions. The R^2 is 0.15521. [A] Regression is low in this case because the accuracy of the NIHSS measured at 6-months post-stroke is questionable. It evaluates the patient based on physical and observable traits. It fails to account for the recovery within the brain. [B] The training set has a R^2 of 0.66106. To a certain extent, the model was able to pair the input to an expected output. However, the overall R^2 indicates that the expected output and target set were not great matches. [Plots from MATLAB Neural Network Fitting Tool.]

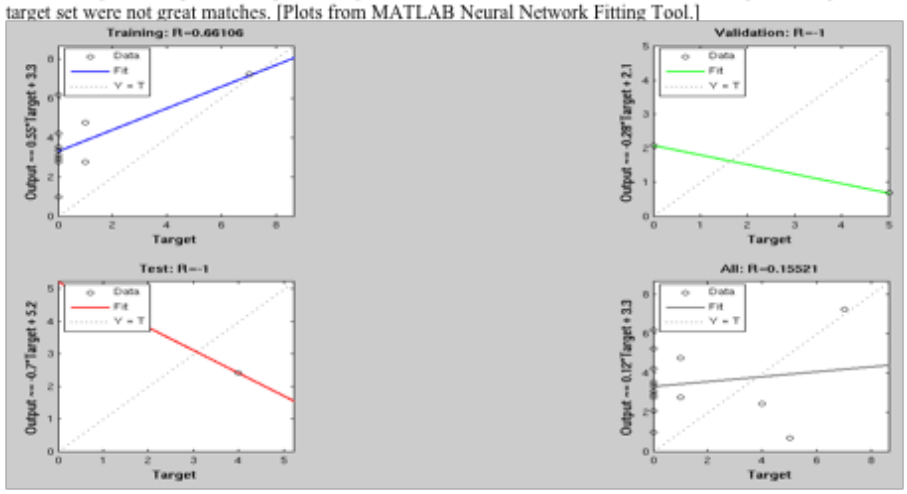

FIGURES 5 THROUGH 9

Discussion

I. Limitations

Because the data did not account for any important medical information like age, gender, etc., this may have resulted in a higher MSE value. In addition, only datasets of 16 patients were used. In the future, it is best to expand the sample size.

ANNs are also sensitive to outliers. Outliers show an effect on MSE, R2, and the overall performance of the model.

Another limitation is the training time of the network. Backpropagation networks tend to train slower than other networks.

Conclusion

This research successfully used MATLAB's Neural Network Fitting Tool to predict stroke recovery from baseline neuroimaging measures. This technique can be used to create accurate predictions of stroke recovery and inform rehabilitation plans for stroke recovery.

Future Works

Based on this research, ANNs are powerful tools in forecasting stroke recovery. The next step of this project is to test it clinically. In the next stage, it is important to account for the patient's history. This can strongly supplement forecasting stroke recovery. The data gathered will be a qualitative measure from the NIHSS, similar to the datasets in this research. However, this trial work will not consist of a 6-month post-stroke dataset. This is where the success of ANNs becomes important. Based on the NIHSS measure of the stroke, physicians can use the ANN to predict the patient's recovery. Medical professionals can then direct the patient's rehabilitation procedures to meet his or her needs. To measure the success of these trials, data will be collected from each patient in 6-months post-stroke. It will compare the data acquired then to the predicted data at the beginning. If both datasets show a close relationship, or the recovery is progressing as expected, this research will be a major breakthrough for clinical practice. By then, it can be concluded that ANNs should be incorporated in clinical and rehabilitation stroke use. This tool essentially has the power to forecast how well the patient will recover and target the appropriate steps to take to recover effectively.

Acknowledgements

This research was supported by Dr. Amy Kuceyeski (Ph.D. Assistant Professor of Mathematics and Neuroscience) of Weill Cornell Medicine's Feil Family Brain and Mind Research Institute. I would like to thank Dr. Kuceyeski for giving insight and expertise in this area of neuroscience, assisting my research, and commenting on my report.

I thank McGill University for permitting the use of the public and unidentified stroke subject data.

References

Tutorialspoint MATLAB Graphics. (n.d.). MATLAB Graphics. Retrieved September 13, 2016, from http://www.tutorialspoint.com/matlab/matlab_graphics.htm

Fit Data with a Neural Network. (n.d.). Retrieved September 13, 2016, from http://www.mathworks.com/help/nnet/gs/fit-data-with-a-neural-network.html

Mupad Transpose. (n.d.). Retrieved September 13, 2016, from http://www.mathworks.com/help/symbolic/mupad_ref/transpose.html

Matrices and Array Indexing. (n.d.). Retrieved September 13, 2016, from http://www.mathworks.com/help/matlab/learn_matlab/matrices-and-arrays.html

Creating and Concatenating Matrices. (n.d.). Retrieved September 13, 2016, from http://www.mathworks.com/help/matlab/math/creating-and-concatenating-matrices.html

Matrix Indexing in MATLAB. (n.d.). Matrix Indexing in MATLAB. Retrieved September 13, 2016, from http://www.mathworks.com/company/newsletters/articles/matrix-indexing-in-matlab.html

MATLAB Matrics. (n.d.). MATLAB Matrix. Retrieved September 13, 2016, from http://www.tutorialspoint.com/matlab/matlab_matrics.htm

MATLAB. (n.d.). Retrieved September 13, 2016, from http://www.mathworks.com/help/matlab/ref/for.html

Loop Control Statements. (n.d.). Retrieved September 13, 2016, from http://www.mathworks.com/help/matlab/matlab_prog/loop-control-statements.html

How Do I Create a for loop in MATLAB. (n.d.). Retrieved September 13, 2016, from https://www.mathworks.com/matlabcentral/answers/31156-how-do-i-create-a-for-loop-in-matlab

MATLAB Lesson for loop. (n.d.). Retrieved September 13, 2016, from http://cse.unl.edu/~sincovec/Matlab/Lesson 08/CS211 Lesson 08 - For Loops.htm

Fit Data with a Neural Network. (n.d.). Retrieved September 13, 2016, from http://www.mathworks.com/help/nnet/gs/fit-data-with-a-neural-network.html

Neural Network Toolbox. (n.d.). Retrieved September 13, 2016, from http://www.mathworks.com/products/neural-network/

Random Number Generation. (n.d.). Retrieved September 13, 2016, from http://www.mathworks.com/help/matlab/random-number-generation.html

Introduction to Vectors in Matlab. (n.d.). Retrieved September 13, 2016, from http://www.cyclismo.org/tutorial/matlab/vector.html

Control. (n.d.). Retrieved September 13, 2016, from http://www.cyclismo.org/tutorial/matlab/control.html

Reshape. (n.d.). Retrieved September 13, 2016, from http://www.mathworks.com/help/matlab/ref/reshape.html

Length. (n.d.). Retrieved September 13, 2016, from http://www.mathworks.com/help/matlab/ref/length.html

Fit Data with a Neural Network. (n.d.). Retrieved September 13, 2016, from http://www.mathworks.com/help/nnet/gs/fit-data-with-a-neural-network.html

Size. (n.d.). Retrieved September 13, 2016, from http://www.mathworks.com/help/matlab/ref/size.html

Train. (n.d.). Retrieved September 13, 2016, from http://www.mathworks.com/help/nnet/ref/trainlm.html

Yu, H., & Wilamowski, B. M. (n.d.). Levenberg–Marquardt Training.

Nonlinear Least Squares Regression Curve Fitting. (n.d.). Retrieved September 13, 2016, from http://www.mathworks.com/help/optim/nonlinear-least-squares-curve-fitting.html

Vectors, Matrices, and Arrays: Size, Length, and Subscripts. (n.d.). Retrieved September 13, 2016, from

http://www.astro.umd.edu/~cychen/MATLAB/ASTR310/vectors02.html

Stroke Recovery. (2015). Retrieved September 13, 2016, from http://www.stroke.org/we-can-help/survivors/stroke-recovery

Updated by: Daniel Kantor, MD, Kantor Neurology, Coconut Creek, FL and Immediate Past President of the Florida Society of Neurology (FSN). Review provided by VeriMed Healthcare Network. Also reviewed by David Zieve, MD, MHA, Isla Ogilvie, PhD, and the A.D.A.M. Editorial team. (2015). Recovering after stroke: MedlinePlus Medical Encyclopedia. Retrieved September 13, 2016, from https://medlineplus.gov/ency/article/007419.htm

About Stroke. Retrieved September 13, 2016, from http://www.strokeassociation.org/STROKEORG/AboutStroke/About-Stroke_UCM_308529_SubHomePage.jsp

NIH Stroke Scale International. (n.d.). Retrieved September 13, 2016, from http://www.nihstrokescale.org/

Abstract W P387: Neurological Correlates Of Brain Function After Acute Stroke--A Dense Array EEG Study. (n.d.). Retrieved September 13, 2016, from http://stroke.ahajournals.org/content/46/Suppl_1/AWP387

The relation between structural and functional connectivity patterns in complex brain networks. (n.d.). Retrieved September 13, 2016, from http://www.ncbi.nlm.nih.gov/pubmed/25678023

A Step by Step Backpropagation Example. (2016). A Step by Step Backpropagation Example. Retrieved September 13, 2016, from https://mattmazur.com/2015/03/17/a-step-by-step-backpropagation-example/

Neural Networks. (n.d.). CHAPTER 2. Retrieved September 13, 2016, from http://neuralnetworksanddeeplearning.com/chap2.html

Nonlinear Least Squares Regression. (n.d.). Retrieved September 13, 2016, from http://www.itl.nist.gov/div898/handbook/pmd/section1/pmd142.htm

Human Connectome Project. (n.d.). Retrieved September 13, 2016, from http://www.humanconnectomeproject.org/

NIH Stroke Scale. (n.d.). NIH Stroke Scale/Score (NIHSS) - MDCalc. Retrieved September 13, 2016, from http://www.mdcalc.com/nih-stroke-scale-score-nihss/

What is the difference between correlation and linear regression? (n.d.). Retrieved September 13, 2016, from http://www.graphpad.com/support/faqid/1141/

Regression and correlation analysis. (n.d.). Retrieved September 13, 2016, from http://abyss.uoregon.edu/~js/glossary/correlation.html

By Michael Nielsen / Jan 2016. (n.d.). CHAPTER 1. Retrieved September 13, 2016, from http://neuralnetworksanddeeplearning.com/chap1.html

Neural Networks - Applications. (n.d.). Retrieved September 13, 2016, from https://cs.stanford.edu/people/eroberts/courses/soco/projects/2000-01/neural-networks/Applications/index.html

On inferring structural connectivity from brain functional-MRI data. (n.d.). Retrieved September 13, 2016, from https://arxiv.org/abs/1502.06659

CS231n Convolutional Neural Networks for Visual Recognition. (n.d.). Retrieved September 13, 2016, from http://cs231n.github.io/neural-networks-1/

Tan, P., Steinbach, M., & Kumar, V. (2005). Introduction to data mining. Boston: Pearson Addison Wesley.

Using the NIHSS: What Are Its Benefits and Pitfalls? (n.d.). Retrieved September 15, 2016, from http://clinicalphysician.net/ebm/using-the-nihss-what-are-its-benefits-and-pitfalls-916.html

Auckland, T. U. (n.d.). Stroke recovery can be predicted. Retrieved September 15, 2016, from http://www.sciencealert.com/stroke-recovery-can-be-predicted

A New Method for Predicting Recovery After Stroke. (n.d.). Retrieved September 15, 2016, from http://stroke.ahajournals.org/content/32/12/2867.full

A Basic Introduction To Neural Networks. (n.d.). Retrieved September 15, 2016, from http://pages.cs.wisc.edu/~bolo/shipyard/neural/local.html

Usability Testing of a Web-Based Decision Aid for Breast Cancer Risk Assessment Among Multi-Ethnic Women

Shayan Huda Chowdhury

Background

Chemoprevention with antiestrogens such as tamoxifen and raloxifene could decrease the incidence of invasive breast cancer among women with high-risk of breast cancer by a staggering 30-70%, similar to the risk reduction of heart diseases. And yet, the adoption of such treatment is abysmally low, to the tune of 5%, with a major reason being lack of awareness among the target beneficiaries about the benefits of chemoprevention, lack of routine breast cancer assessment and lack of knowledge about chemoprevention leading to concerns about its side effects, due to it being associated with those of chemotherapy.

Methods

Dr. Katherine Crew's team has developed RealRisks, a web-based patient decision aid (PtDA) to facilitate informed decision-making about chemoprevention by communicating eachpatient's individual risk of breast cancer using their own personal information regarding family and medical history. The purpose of this research is to understand usability issues of RealRisks among patients of different ethnic, economic and educational backgrounds, ages, and English proficiencies. The hypothesis is that such factors will significantly affect the subject's ability to use RealRisks and thus influence adoption of chemoprevention.

Results

In-depth analysis of the study's findings suggested that user behavior using surveys, usability recordings, ease of use and navigability of the tool, etc. may make improvements in the content and thus lead to increased adoption. Over 85% of the participants thought that RealRisks was useful and easy to use, while others alluded that it had limitations, which helped identify most of the various usability concerns regarding the tool.

Conclusions

Most notable of these concerns were those relating to the childish undertones of the light and dense narratives and the confusion aroused in the study volunteers by the risk games and the comprehensive action plan, generated after all the seven modules of the decision aid are completed. Improvements were made and resulting findings suggested that such developments had a tremendous effect on usability for the target demographic. Larger implications of this research are that the study underscores importance of usability testing in creating culturally relevant and thus, targeted patient decision aids designed for diverse populations with varying health literacy and acculturation.

Regulation of Skeletal Fracture Angiogenesis by Immune-Derived Paracrine Secretions

Constantine Athanitis

Annotated by Heyu Li

Abstract Many mechanisms are activated during skeletal fracture repair, including angiogenesis, osteogenesis, and the inflammatory response. While the individual events are known, the interplay of the inflammatory responses and angiogenesis are not completely understood. We hypothesize that the early inflammatory response facilitates angiogenesis through the upregulation of cytokines. Due to the inherent flaws of purely *in-vivo* or *in-vitro* studies, we have developed a combination of the two, creating a 3D biomimetic angiogenesis model to study the interactions of the cytokines on C166-GFP endothelial cells within the engineered microenvironment. As a result of complex cytokine behaviors and effects, we tested different concentrations and times of TNF-alpha, IL-1beta, and IL-6. The angiogenic sprouting length and frequency increased in the presence of cytokine conditioned media (CM).

Generation of new blood cells

General term for small proteins that are used in cell communication in immune responses, or urges cells to move to certain locations in pathways of immune response. The main distinction between cytokines is that the concentration magnitude of cytokines never fluctuate by more than one order, while cytokines can increase by 1000 fold. Also, cytokines can affect the cell that secretes them along with others.

Introduction

For decades, there have been two main ways to study and analyze biological mechanisms: *in-vivo* and *in-vitro*. Each has its own advantages and disadvantages. *In-vivo* studies are those that are tested on living organisms and are advantageous because any effects observed in the study show how an actual organism's body will respond to the experiment or treatment. The downside is having to address any moral and ethical dilemmas. For this reason, we used a new design for a two-layered 3-D microfluidic device. These devices integrate a 3-Dimensional collagen scaffold with two micro-channels (400 μm) to allow for not only the complete control of the cells' physical environment, as in a 2-D *in-vitro* device, but also for the extraction of solutes, growth of endothelial cells, delivery of circulating cells, and control of mechanical factors such as wall tension and shear stress.1 Angiogenesis is the formation of new blood vessels from preexisting vessels, involving the migration, growth, and differentiation of endothelial cells. This process ensures that all metabolically active cells receive their necessary biochemical factors. Our project focuses on the immune-angiogenesis crosstalk during fracture repair. Angiogenesis is tied with bone repair, since nutrients such as oxygen, growth factors, cytokines, osteoblast and osteoclast precursors require a vascular route to reach the injury site for acute treatment. Within the first day of bone fracture, a hematoma (or a solid swelling of clotted blood) forms at the site to prevent the loss of blood and chemical factors.2 An acute inflammatory response arises to coagulate the hematoma in between the two fractured bone ends and to release proinflammatory cytokines, signaling molecules, adjacent to the injury site. It is known proinflammatory cytokines have degradative effects for bone tissue when exposed long-term.3 Smacrophages are Tumor Necrosis Factor (TNF-a), Interleukin-1, 6, 11, and 18, platelet-derived growth factor, vascular endothelial growth factor (VEGF), and bone morphogenetic protein.

Devices that precisely control the movement of fluids in a very small space, in this case to replicate angiogenesis.

Stress arising from friction between fluid particles.

Linked to brain metastases and other forms of cancer. Is found to be upregulated.

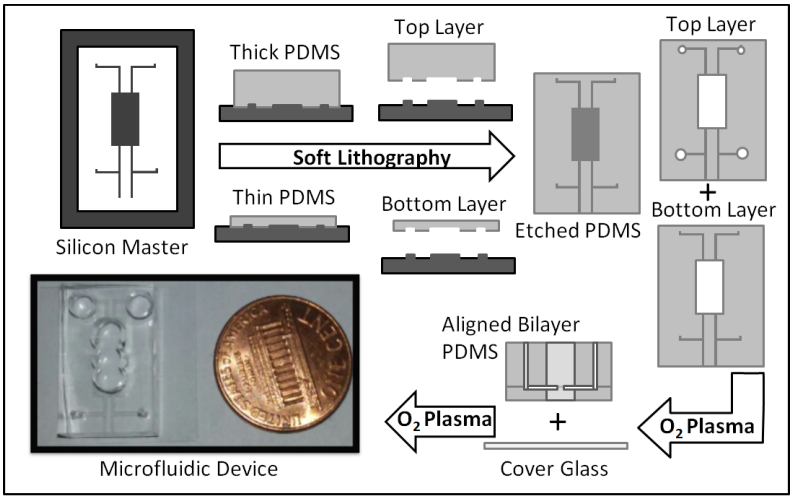

Fig. 1 Schematic of Microfluidic Manufacturing Process. Uncured 10:1 PDMS is poured over SU-8 Silicon Master wafer to create a thick and thin PDMS layer. After curing in an 80 degree Celsius oven, the PDMS is etched with the necessary channels via soft lithography. A two tiered microfluidic device was fabricated as a scaffold to mimic the three-dimensional geometry of blood vessels. A 10:1 solution of Polydimethylsiloxane (PDMS) and curing agent (Dow, Midland, MI) was made and poured over a photoresist SU-8 silicon wafer to create thick and thin layers. These layers were then finally bonded together via oxygen plasma treatment.

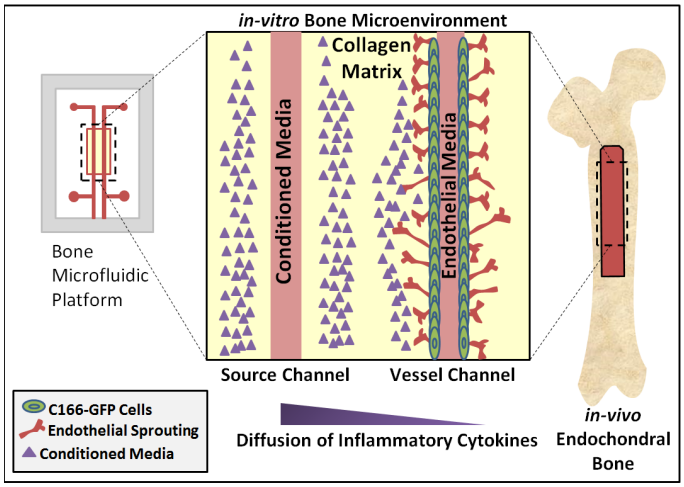

Fig. 2 Biomimicry of Bone Fracture Site. One of the parallel channels mimics a blood vessel located at the fracture site, while the other channel mimics the source of cytokine factors from nearby cells.

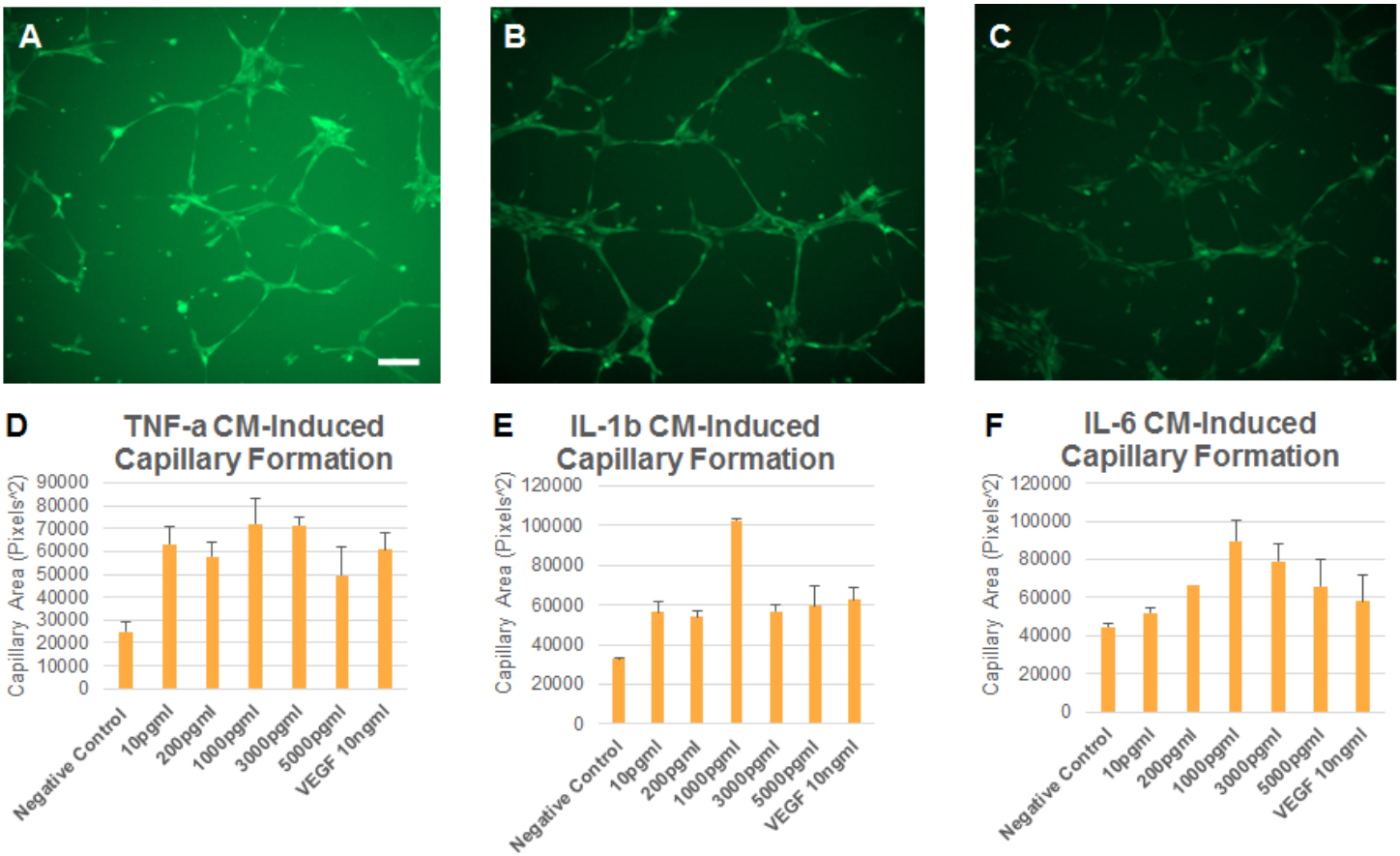

Fig. 3 Capillary Tube Formation Assay to screen optimal concentrations of TNF-alpha, IL-1beta, and IL-6. (A) Tubule formation for cells supplied with TNF-alpha 3000pg/mL. (B) Tubule formation for cells supplied with IL-1beta 1000pg/mL. (C)Tubule formation for cells supplied with IL-6 1000pg/mL. (D)Compared to the negative control, all concentrations of TNF-alpha showed a relatively large increase in capillary area. 1000pg/mL and 3000pg/mL seem to be the most effective concentrations. (E) While all concentrations of IL-1beta induced higher capillary areas than the negative control, 1000pg/ml had the biggest difference. (F) The IL-6 concentrations appear to have a bell-curve effect on capillary area. As the concentration increases to 1000pg/mL, the area increases as well. After that concentration however, the area decreases. Data are represented as Mean+/-Standard Deviation. Scale Bar = 100um.

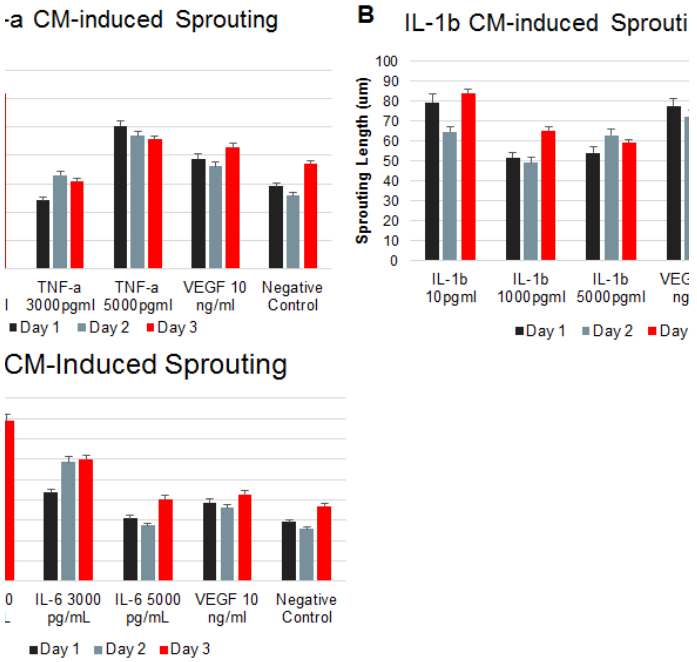

Fig. 4 CM-Induced Sprouting caused by IL-6, IL-1beta, and TNF-alpha. (A) All concentrations of IL-6 produced sprouts longer than the negative control, but 5000 pg/mL was not better than the VEGF, or positive control, that we used. It seems that the lowest concentration, 10 pg/mL was the most effective(B) In contrast to A, 10 pg/mL of IL-1beta was the only concentration to be more effective than the negative control. Even then, VEGF was better in both days 2 and 3. (C) TNF-alpha also produced considerably long sprouts. Although 3000 pg/mL was the least effective out of the rest of the concentrations, 5000 pg/mL was still better than both positive and negative controls. Overall IL-6 produced the longest sprouting lengths, while TNF-alpha and IL-1beta came in second and last, respectively.

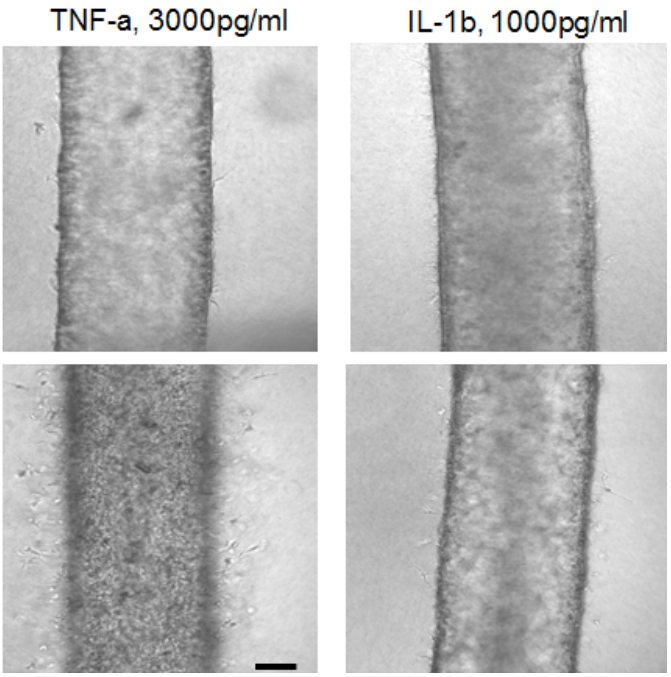

Fig. 5 Brightfield images of Day 0 and Day 3. The images show the difference in sprouting lengths, on the left side of each vascular channel, for 10 ng/mL of positive control, and 10 pg/mL of the three types of conditioned media, which was the most effective concentration for all of them. Day 0 shows relatively no sprouting growth, just normal vascular vessel protrusions. Day 3 shows the maximum growth of individual sprouts. Scale bar = 100um. In respect to the three-dimensional sprouting formation, the most effective concentration of each cytokine was 10 pg/mL. For IL-1beta, VEGF was more effective in creating longer sprouts when compared to 10 pg/mL of the cytokine. It seems that for all of the cytokines, as the concentration increases, the sprouting length decreases. This must mean that the most effective range of all cytokines falls in from 5 pg/mL to 1000 pg/mL

Discussion

The inflammatory response is an important modulator for signalling recruited cells into the bone fracture microenvironment. This study has shown that concentration-specific paracrine cytokines have a proangiogenic effect which may modulate the angiogenesis in bone repair.

Cytokines that only have effect in the cells surrounding the cell producing the protein.

From previous studies, it has been indicated that low concentrations of TNF-alpha promote angiogenesis, while high concentrations of TNF-alpha inhibit it.8 Due to this dual-nature of cytokine behavior, our study has screened that the optimal proangiogenic cytokine concentrations are closer to 10pg/mL for endothelial sprouting. However, our tubule formation assay indicates otherwise, resulting in an optimal concentration of 1000-3000pg/mL for all tested cytokines. This discrepancy may be a result of two different processes: angiogenesis and vasculogenesis.

From previous studies, it has been indicated that low concentrations of TNF-alpha promote angiogenesis, while high concentrations of TNF-alpha inhibit it.8 Due to this dual-nature of cytokine behavior, our study has screened that the optimal proangiogenic cytokine concentrations are closer to 10pg/mL for endothelial sprouting. However, our tubule formation assay indicates otherwise, resulting in an optimal concentration of 1000-3000pg/mL for all tested cytokines. This discrepancy may be a result of two different processes: angiogenesis and vasculogenesis.

Conclusion and Future Work

With respect to the creation and fabrication of the microfluidic devices, the two main limitations are time and accuracy. This time limit results in fewer devices being made, which then results in fewer experiments being made. Since our research involves endothelial cells, once experiments have started, they must be constantly upheld in order to use the cells. If not enough devices are made in time, the cells will not be able to be used in the current round of experiments. Additionally, the devices are made manually. Therefore, without the help of a machine, manually combining the device layers together proves to be less precise due to incomplete and inaccurate alignment.

For both of these reasons, our group hopes to acquire and use a 3D printer to fabricate the devices. A stereolithography (SLA) or Digital Micrometer Device-based Projection (DMD-P) printer will do.7 By using a 3D printer, we will be able to mass produce the devices in near perfection, cutting down production time at the same time. Another limitation of this project is the imaging and quantification. Firstly, our microscope takes images in two dimensions. The problem with this is that the angiogenic sprouts grow all over the three dimensional vessels. As a result, we can't accurately observe, record, and quantify all sprouts. Also, because the cells are not confined to the boundaries of the collagen vessel, the walls of the cell vessels aren't necessarily uniform. Thus, quantification of certain sprout lengths is arbitrary, since they would each have a unique base on the vessel. In addition to making this experiment's process more efficient, I also hope to continue exploring the bone repair mechanism by doing more research on mesenchymal stem cells' role in it. I would create a new microfluidic design with three channels to mimic the bone microenvironment specifically in the MSC's perspective. That is to say, one channel will act as the bone marrow where MSCs are stored, the middle channel will act as the fracture or hematoma site, and the third channel will act as the vasculature that contains cytokines and other factors. By using this design, I would be able to investigate how cytokines released during the inflammatory response of the bone repair affect MSC migration and differentiation.

A type of precise 3D printing that uses light to fuse ink molecules together.

You could use mCherry to track the movement of fluids and then use some form of 3d light spectrometry to see the results. This might provide better results.

References

Stroock, A. D., Ph, D., Fischbach, C., & Ph, D. (2010). Microfluidic Culture Models of Tumor Angiogenesis, 16 (7).

Tsiridis, E., Upadhyay, N., & Giannoudis, P. (2007). Molecular aspects of fracture healing: which are the important molecules? Injury, 38 Suppl 1(1), S11-25. http://doi.org/10.1016/j.injury.2007.02.006

Marsell, Richard, and Thomas A. Einhorn. “THE BIOLOGY OF FRACTURE HEALING.” *Injury* 42.6 (2011): 551–555. *PMC*. Web. 13 Sept. 2016.

Wang, X., Wang, Y., Gou, W., & Lu, Q. (2013). Role of mesenchymal stem cells in bone regeneration and fracture repair : a review, (28), 2491–2498.

Adair TH, Montani JP. Angiogenesis. San Rafael (CA): Morgan & Claypool Life Sciences; 2010. References.Available from: http://www.ncbi.nlm.nih.gov/books/NBK53239/

Liu, C., Cui, X., Ackermann, T. M., Flamini, V., Chen, W. and Castillo, A. B. (2016). Osteoblast-derived paracrine factors regulate angiogenesis in response to mechanical stimulation. *Integrative Biology*. http://doi.org/10.1039/C6IB00070C

Ho, C. M. B., Ng, S. H. G., Li, K. H. H., & Yoon, Y.-J. (2015). 3D Printed Microfluidics for Biological Applications. *Lab Chip*, *15*(3), 3627–3637. http://doi.org/10.1039/C5LC00685F

Fajardo LF, Kwan HH, Kowalski J, Prionas SD, Allison AC. Dual role of tumor necrosis factor-alpha in angiogenesis. *Am J Pathol.*1992;140:539–44.

CONTACT US

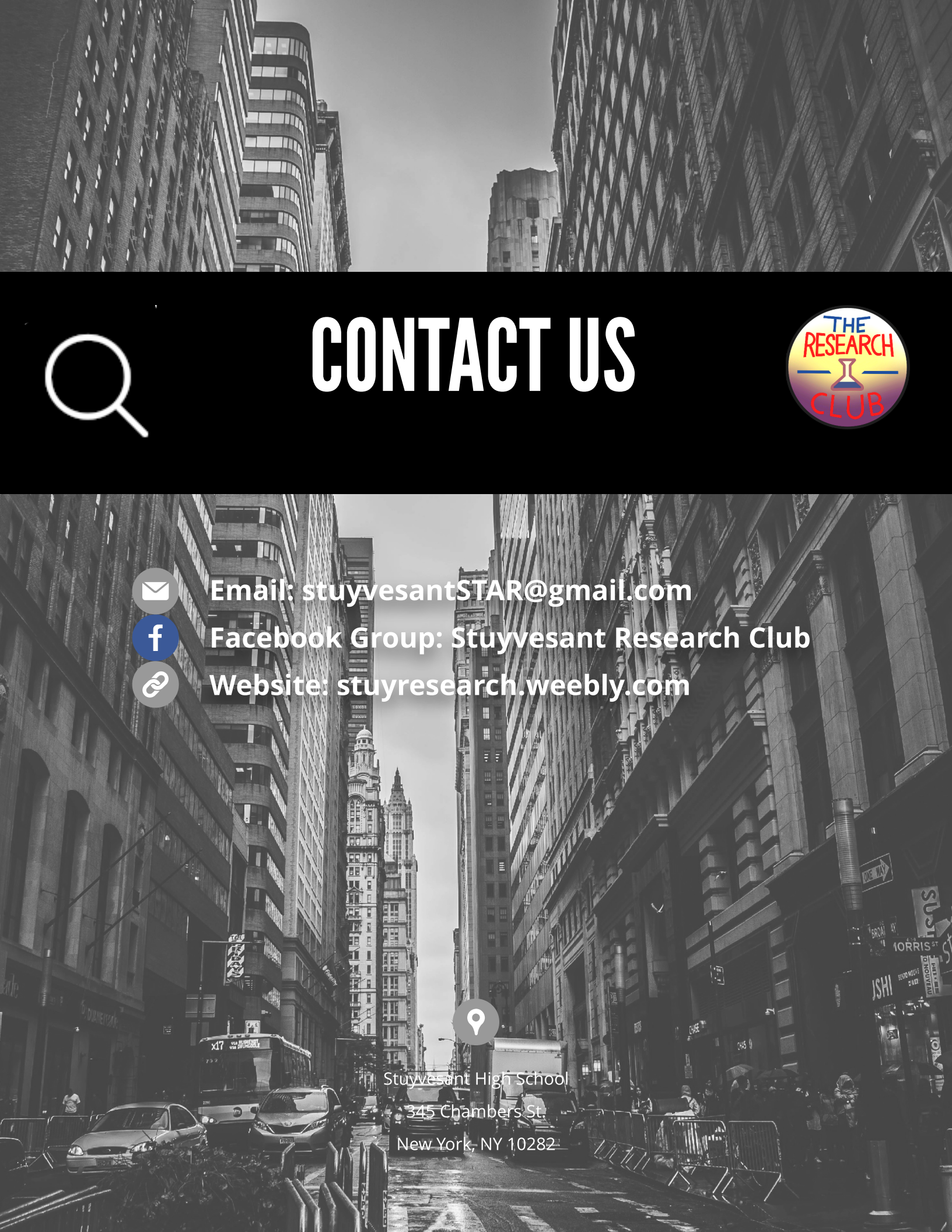

Email: stuyvesantSTAR@gmail.com

Facebook Group: Stuyvesant Research Club

Website: stuyresearch.weebly.com

Stuyvesant High School

345 Chambers St.

New York, NY 10282